Engineering Alkane-Inducible Fimbriation in *Escherichia coli*

A Thesis

Presented to

the Faculty of the Department of Chemical and Biomolecular Engineering

University of Houston

In Partial Fulfillment

of the Requirements for the Degree

Master of Science

in Chemical Engineering

by

Ryan B. McLay

May 2016

Engineering Alkane-Inducible Fimbriation in *Escherichia coli*

Ryan B. McLay

Approved:

Co-Chair of the Committee:
Dr. Jacinta C. Conrad
Associate Professor, Department of
Chemical & Biomolecular Engineering

Co-Chair of the Committee:
Dr. Patrick C. Cirino
Associate Professor, Department of
Chemical & Biomolecular Engineering

Committee Members:

Dr. Debora F. Rodrigues,
Assistant Professor, Department of
Civil & Environmental Engineering

Dr. Suresh K. Khator, Associate Dean
Cullen College of Engineering

Dr. Michael P. Harold, Chair
Dept. of Chemical & Biomolecular Eng.

Acknowledgments

I would like extend my greatest gratitude and thanks to my Master's Thesis advisors, Dr. Jacinta C. Conrad and Dr. Patrick C. Cirino, for their support and guidance. I would like to also thank everyone in Dr. Cirino's lab at the University of Houston for their pragmatic inputs and discussions, especially Shuai Qian who taught me all molecular biology lab techniques I applied in my research. Lastly, I would like to thank all my friends and family for their love and encouragement throughout my graduate studies.

Engineering Alkane-Inducible Fimbriation in *Escherichia coli*

An Abstract

of a

A Thesis

Presented to

the Faculty of the Department of Chemical and Biomolecular Engineering

University of Houston

In Partial Fulfillment

of the Requirements for the Degree

Master of Science

in Chemical Engineering

by

Ryan B. McLay

May 2016

Abstract

Fimbriae are small, hair-like appendages arranged on many bacteria's outer-membrane surfaces used for binding to biotic and abiotic surfaces to resist shear forces and attach to nutrient sources. Fimbriae are important in the initial attachment of cells to a substrate as well as the subsequent irreversible attachment to a surface. In this investigation, *E. coli* was engineered to over-express fimbriae in response to the presence of IPTG and DCPK. The over-expression of fimbriae in *E. coli* resulted in a pronounced response to the agglutination of mannose-containing yeast cells, causing them to sediment from solution at a much faster rate than wild-type or fimbrial deletion strains. Furthermore, the presence of fimbriae resulted in a significantly higher partitioning of cells into hydrocarbon sources across a range of alkanes. Lastly, the presence of fimbriae was shown to be essential in the development of biofilms, where only strains expressing fimbriae resulted in biofilm formation.

Table of Contents

Acknowledgments ..... **v**

Abstract ..... **vii**

Table of Contents ..... **viii**

List of Figures ..... **xi**

Chapter 1 Introduction **1**

1.1 Fimbriae and Biofilms 1

1.2 Implications in Bioremediation: 3

Chapter 2 Background **5**

2.1 Structure and Genetic Organization of Fimbriae 5

2.2 FimH Binding "Pocket" for Attachment to Biotic and Abiotic Surfaces 6

2.3 Remediation Techniques 10

2.4 Engineered Species for Bioremediation 12

Chapter 3 Experimental Methods **15**

3.1 Plasmid Construction 15

3.1.1 pPCC1401 ..... *15*

3.1.2 pPCC1403 ..... *16*

3.1.3 Plasmid History *16*

3.2 Yeast Agglutination Assay/Sedimentation Assay (YAA) 17

3.3 Microbial Adhesion to Hydrocarbons (MATH) Assay 20

3.4 Specific Biofilm Formation (SBF) Assay 22

3.5 Transmission Electron Microscopy (TEM) Imaging 23

Chapter 4 Manipulation of fim Operon for Fimbrial Expression in *Escherichia coli* 26

4.1 Methodology 26

4.1.1 Materials *26*

4.1.2 Preparation *26*

4.2 Assays and Characterization 27

4.2.1 Yeast Agglutination and Sedimentation Assay (YAA) *27*

4.2.2 Microbial Adhesion to Hydrocarbon Assay (MATH) *33*

4.2.3 Specific Biofilm Formation (SBF) *37*

4.2.4 Transmission Electron Microscopy (TEM) Imaging *40*

4.3 Discussion 41

4.4 Conclusion 45

Chapter 5 Alkane-Inducible Fimbriation for Bioremediation Processes 46

5.1 Methodology 46

5.1.1 Materials *46*

5.1.2 Preparation *46*

5.2 Assays and Characterization 47

5.2.1 Yeast Agglutination and Sedimentation Assay (YAA) *47*

5.2.3 Specific Biofilm Formation (SBF) *52*

5.3 Results and Discussion 55

5.4 Conclusion 60

Chapter 6 Conclusion 62

6.1 Summary and Conclusion 62

6.2 Future Work 64

6.2.1 Chemotaxis towards Environmental Contaminants 65

6.2.2 Metabolism of Environmental Contaminants 66

References 68

List of Figures

Figure 1: Invertible "fim switch" element responsible for turning on/off fimbrial expression.25 5

Figure 2: Visual representations of (A) assembled fimbrial unit and (B) fimbrial tip housing FimH.27,26 6

Figure 3: The fimbrial tip is composed of (A) two domain lectin and pilin protein containing (B) the mannose-binding pocket (yellow) at fimbrial tip responsible for attachment of fimbriae to surfaces.32 7

Figure 4: Hydrophobic "tyrosine gate" flanks the mannose binding pocket to mediate binding of mannose-containing groups to the FimH adhesin.12,34,35 9

Figure 5 Superfund source treatment projects by category.42 10

Figure 6: Yeast Agglutination and Sedimentation Assay 18

Figure 7: Surface Coverage of Fimbrial Adhesive Tips (FimH) by Methyl-α-D-Pyrannoside. 19

Figure 8: Methyl-α-D-Pyrannoside Mechanism of Inhibition for the Agglutination of Yeast Cells. 19

Figure 9: The FimH adhesin is responsible for binding of *E. coli* to yeast cells. 20

Figure 10: Microbial Adhesion to Hydrocarbon (MATH) Assay. 21

Figure 11: Visualization of MATH assay with increasing level of partitioning to hydrocarbon phase with increasing level of fimbrial expression. 22

Figure 12: Biofilm formation increases with increasing level of fimbriation. From left to right (periphery wells left blank): LB only, 1401- (0.0 mM IPTG + glucose), 1401+ 1.0 mM IPTG, MG1655, MG1655ΔfimA. 23

Figure 13: Yeast agglutination assay (YAA), measuring absorbance as a function of time for *E. coli* strain MG1655 with and without addition of IPTG for mixing times of (A) 3 hours and (B) 36 hours. IPTG addition did not result in any increase in sedimentation rate. 28

Figure 14: Yeast agglutination assay (YAA), measuring absorbance as a function of time for *E. coli* strain MG1655ΔfimA with and without addition of IPTG for mixing times of (A) 3 hours and (B) 36 hours. IPTG addition did not result in an increased sedimentation rate. 29

Figure 15: Yeast agglutination assay (YAA), measuring absorbance as a function of time for *E. coli* strain MG1655ΔfimA-pPCC1401 with and without addition of IPTG for mixing times of (A) 3 hours and (B) 36 hours. The addition of IPTG resulted in a dramatic increase in the rate of sedimentation.....30

Figure 16: Yeast agglutination assay (YAA), measuring absorbance as a function of time for *E. coli* strain MG1655ΔfimA-pFG1 with and without addition of IPTG for mixing times of (A) 3 hours and (B) 36 hours. IPTG addition did not result in any increase in the sedimentation rate.....31

Figure 17: Yeast agglutination assay (YAA), measuring absorbance as a function of time for all *E. coli* strain tested with and without addition of IPTG for mixing times of (A) 3 hours and (B) 36 hours. The addition of IPTG in MG1655ΔfimA-pPCC1401 resulted in a dramatic increase in the rate of sedimentation, while wild-type MG1655 displayed a moderate sedimentation rate.....32

Figure 18: Microbial Adhesion to Hydrocarbon (MATH) Assay in hexane, measuring absorbance as a function of microbial hydrophobicity in ΔfimA, MG1655,

pPCC1401 without induction, pPCC1401 with induction. Engineered strain MG1655ΔfimA-pPCC1401 partitioned into the hydrocarbon phase at the highest rate. 34

Figure 19: Microbial Adhesion to Hydrocarbon (MATH) Assay in dodecane, measuring absorbance as a function of microbial hydrophobicity in ΔfimA, MG1655, pPCC1401 without induction, MG1655ΔfimA-pPCC1401 with induction. Engineered strain MG1655ΔfimA-pPCC1401 partitioned into the hydrocarbon phase at the highest rate. 35

Figure 20: Microbial Adhesion to Hydrocarbon (MATH) Assay in hexadecane, measuring absorbance as a function of microbial hydrophobicity in ΔfimA, MG1655, pPCC1401 without induction, pPCC1401 with induction. Engineered strain MG1655ΔfimA-pPCC1401 partitioned into the hydrocarbon phase at the highest rate. 36

Figure 21: Microbial Adhesion to Hydrocarbon (MATH) Assay in toluene, measuring absorbance as a function of microbial hydrophobicity in ΔfimA, MG1655, pPCC1401 without induction, pPCC1401 with induction. Engineered strain MG1655ΔfimA-pPCC1401 partitioned into the hydrocarbon phase at the highest rate. 36

Figure 22: 96-well plate biofilm formation assay, measuring the absorbance of crystal violet (CV) stained biofilms as a function of time. For each sample, biofilm absorbance was measured at 12 h (sparsely shaded), 24 h (medium shading), and 48 h (dense shading). The engineered strain MG1655ΔfimA-pPCC1401 developed the highest amount of biofilm. 38

Figure 23: Specific Biofilm Formation (SBF) assay, measuring the absorbance of crystal violet stained biofilms as a function of time and semi-normalized to bacterial growth. For each sample, SBF absorbance was measured at 12 h (sparsely shaded), 24 h (medium shading), and 48 h (dense shading). The engineered strain MG1655ΔfimA-pPCC1401 developed a much higher SBF than all controls. 39

Figure 24: Transmission electron micrographs of induced MG1655ΔfimA-pPCC1401 (left, engineered strain), MG1655 (center, wild-type), and MG1655ΔfimA (right, fimbrial deletion). The engineered strain MG1655ΔfimA-pPCC1401 displayed many more fimbriae than wild-type MG1655, while MG1655ΔfimA displayed no fimbriae. 40

Figure 25: Yeast agglutination assay (YAA), measuring absorbance as a function of time for MG1655ΔfimA-pPCC1401 and dual-inducible expression of fimbriae in MG1655ΔfimA-pPCC1403. The presence of inducers IPTG and DCPK played a large role in the sedimentation rate. 48

Figure 26: Alkane-inducible MG1655ΔfimA-pPCC1403 shows similar agglutinating power to MG1655ΔfimA-pPCC1401, both of which sediment at a faster rate than control strains. 49

Figure 27: Effects of inducers IPTG and DCPK on fimbrial expression in engineered bacteria across separate ranges of inducer concentrations: variable IPTG, no DCPK (A), no IPTG, variable DCPK (B), constant IPTG, variable DCPK (C), and variable IPTG, constant DCPK (D). 51

Figure 28: Biofilm formation quantified by crystal violet staining across three different time points (12, 24, 48 hours) for alkane-inducible MG1655ΔfimA-pPCC1403 compared against controls. 52

Figure 29: Specific biofilm formation normalized to bacterial growth and biofilm staining for alkane-inducible MG1655ΔfimA-pPCC1403 across different time points (12, 24, 48 hours). 53

Figure 30: Effect of glucose addition on biofilm formation for engineered systems of IPTG inducible MG1655ΔfimA-pPCC1401 and dual-inducible MG1655ΔfimA-pPCC1403 (24 hour). 54

Figure 31: Effect of glucose addition on the specific biofilm formation (SBF) of MG1655ΔfimA-pPCC1401 and MG1655ΔfimA-pPCC1403, normalized against cellular growth rate (24 hour). 55

Chapter 1 Introduction

Escherichia coli has been a valuable workhorse for genetic engineering for many decades due to its well established characterization of genetic components. In this investigation, *E. coli* was engineered to over express the cellular surface structure known as fimbriae in response to the presence of model chemicals and hydrocarbons. Fimbriae are essential for initial biofilm development which protects cells in a hazardous environment. By engineering fimbrial expression in *E. coli*, not only will cells stick to areas containing a targeted pollutant, but they will also become protected by the developing biofilm. To this end, yeast agglutination assay (YAA), microbial adhesion to hydrocarbon (MATH) assay, and specific biofilm formation (SBF) assay were used to quantify the level of fimbriation in *E. coli*.

1.1 Fimbriae and Biofilms

Fimbriae are small, hair-like appendages arranged on many bacteria's outer membrane surface and are found in many species. Typically, fimbriae are 7 – 10 nm wide and up to several microns in length.[1–3] These extracellular structures are used to bind to both biotic and abiotic surfaces to anchor cells to surfaces so as to resist shear forces (caused by flow) and to attach to nutrient sources.[4–6] In addition to surface attachment, influence initial cell-to-surface biofilm formation in a range of culture conditions, including both static and flow conditions as well as minimal and rich nutrient/media conditions.[7]

Fimbriae are important in the initial attachment of cells to a substrate as well as the subsequent irreversible attachment to a surface. Irreversible attachment to varying surfaces (biotic or abiotic) is achieved through two primary mechanisms: via surface interactions with specific adhesion groups located at the tip of fimbriae, and especially the tip adhesin

FimH; and through production of extracellular polymer substances (EPS) including exopolysaccharides, proteins, and macromolecules such as DNA and lipids.[8–10] The mechanisms controlling molecular attachment of cells to a substrate through adhesins is not yet fully understood, but is most likely due to the hydrophobic interactions of amino acid (AA) residues located at the fimbrial tip.[11,12,13] Following the initial stages of cellular attachment to a substrate, cells begin to colonize and spread out across a surface. At this point, depending on environmental cues (often via inhospitable changes in the immediate habitat), a complex biofilm architecture begins to emerge as a protection mechanism, complete with water channels, pores, and trapped nutrients in which the encapsulated cells exhibit totally different behavior compared to planktonic (suspended/swimming) cells.[14]

Biofilm formation and maturation has been suggested to occur in at least five distinct stages:[7] Initial cellular attachment to a surface (weak and readily reversible); transition to irreversible attachment (by specific adhesins such as fimbriae/pili or extracellular polymer matrix production); early developmental stage of 3D growth; development of biofilm architecture into mature biofilms; and release of cells following biofilm maturation. The presence of fimbriae has been shown to greatly increase the level of biofilm development in static culture conditions[15], which is almost requisite for development of biofilms. An increase in the level of cellular fimbriation will/should lead to an increase in biofilm formation that will increase the likelihood of cellular survival and proliferation – and thus metabolism of environmental pollutants that would otherwise result in cell death.

1.2 Implications in Bioremediation:

Bioremediation is a broad term encompassing the use of microorganisms to treat contaminated materials, whether liquid or solid, through natural or enhanced biochemical degradation mechanisms present in microbes (including bacteria, yeast, and fungi). Currently, there are more than 1,320 Superfund National Priority List (NPL) sites for hazardous substances, pollutants, or contaminant releases.[16] Not only is the clean-up of contaminated sites a national priority with significant environmental and societal impacts, but remediation of such sites is also a projected hundred billion dollar industry.[17] With their pathways of cellular metabolism extensively characterized and plethora of genetic tools available for the design of novel and targeted cellular properties, *E. coli* is a perfect candidate for engineering bioremediation techniques. The use of engineered bacteria for bioremediation can enhance the specific degradation of environmental contaminants and may be used to remediate soils/liquids. Such treatment may be performed ex situ by removing contaminated material from its native site and treating elsewhere, or in situ by injection wells to introduce biodegrading microorganisms and biostimulants (i.e., pH modulators, moisture, aeration, nutrients) to enhance metabolic or survival rates.[18]

Chemically contaminated industrial areas (such as Superfund sites) contain high concentrations of pollutants that can either inhibit cell proliferation, as characterized by the inhibitory concentration (IC50), to prevent cell proliferation or kill most organisms and cells, as quantified by the lethal dose (LD50). The minimal inhibitory concentration (MIC) is the most commonly used metric to measure cellular sensitivity to an antimicrobial agent (such as an antibiotic) and defines the lowest concentration of a compound that inhibits cellular proliferation across time.[19] However, this metric measures the sensitivity of

planktonic cells; when the MIC metric is applied to cells in a biofilm, it fails to measure the true antibiotic MIC. This discrepancy prompted the development of the minimal biofilm eliminating concentration (MBEC), a new metric that more fully describes the MIC of an antimicrobial agent required to prevent cellular growth.[20,21] Such experiments suggest that biofilms provide one route by which cells resist the toxic effects of many poisons, as the biofilm matrix limits the diffusion of normally toxic chemicals and hence protects individual cells;[20–22] accordingly, biofilms theoretically increase the likelihood of cellular proliferation and growth, thus increasing the speed of remediation. Therefore, an increase in the level of cellular fimbriation should lead to an increase in biofilm formation which will increase the likelihood of cellular survival and proliferation. In turn, when combined with another engineered trait such as metabolism of environmental pollutants, fimbriation will lead to a superior response towards targeted pollutants with a higher efficiency and survival rate.

Chapter 2 Background

2.1 Structure and Genetic Organization of Fimbriae

The *fim* operon is an approximately 10kb pair gene fragment that consists of *fimB, fimE, fimA, fimI, fimC, fimD, fimF, fimG*, and *fimH* genes. Both *fimB* and *fimE* regulate the expression of fimbria in *Escherichia coli*. These genes are site-specific recombinases, enzymes that promote genetic recombination, and mediate fimbriae phase switching from on to off and vice versa.[23] *fimB* can mediate phase switching bi-directionally from phase-ON to phase-OFF as well as phase-OFF to phase-ON; *fimE*. however, can only mediate phase switching uni-directionally from phase-ON to phase-OFF.[24] Both *fimB* and *fimE* are upstream genes to an invertible element, *fimS*, which is responsible for the phase-ON and phase-OFF behavior of bacterial fimbria (Fig. 1).

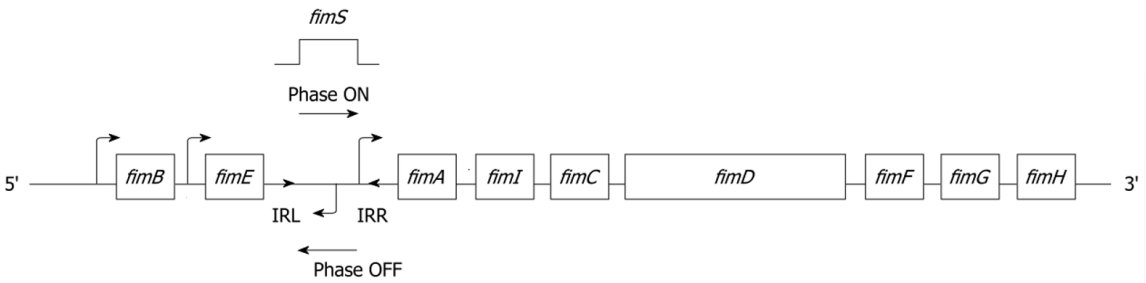

Figure 1: Invertible "fim switch" element responsible for turning on/off fimbrial expression.[25]

The genes involved in the physical construction of fimbria are located downstream of *fimS* in the cluster of genes *fimA-H*. *fimA* is the major structural fimbrial subunit of fimbria; *fimI* is an uncharacterized gene whose function in unknown; *fimH* is an adhesion site responsible for binding, e.g., to receptors containing mannose; and *fimF* and *fimG* compose the small structure tip that houses the *fimH* adhesion gene.[25] *fimC* and *fimD* are involved in the transport and assembly of type 1 fimbriae/pili known as the chaperon-usher pathway; *fimC* facilitates three simultaneous function including folding of subunits,

stabilization of subunits, and capping of subunits in the periplasm whereas *fimD* is an outer-membrane usher that transports fimbria outside of the cell during the nascent construction of fimbria/pilus.[26] The relative physical organization of proteins constituting fimbrial development are shown in Figure 2A, where the majority of the fimbrial structure is related to the FimA major structural protein. Figure 2B visually displays an electron micrograph of the fimbrial tip adhesin, FimH, which is a small but very important component of cellular fimbriae.

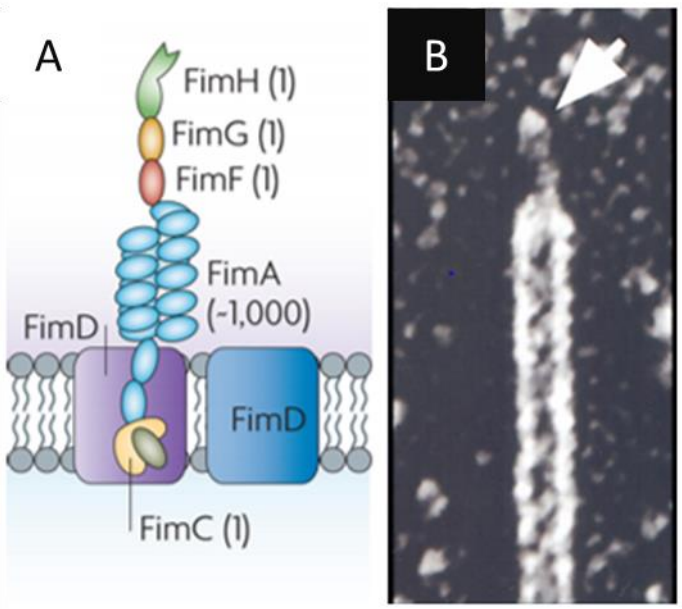

Figure 2: Visual representations of (A) assembled fimbrial unit and (B) fimbrial tip housing FimH.[27,26]

2.2 FimH Binding "Pocket" for Attachment to Biotic and Abiotic Surfaces

The unique binding and attachment properties of fimbriae to biotic and abiotic surfaces result primarily from the FimH binding pocket, located at the distal end of individual fimbria. The FimH binding pocket binds specifically to biotic α-D-mannose containing substrates binds non-specifically to a variety of abiotic surfaces, including polyvinyl chloride (PVC), polycarbonate, polystyrene, and borosilicate glass.[28]

Furthermore, adhesion of FimH to abiotic surfaces has been shown to maintain a similar binding mechanism as does FimH to biotic surfaces; this was shown through addition of methal-α-D-pyrranoside (a non-metabolism analogue of mannose) to cellular suspensions, which prevented biofilm formation on abiotic surfaces.[29]

The FimH protein consists of two domains, a mannose-recognizing lectin and a pilin domain that connects the FimH tail to the rest of the fimbrial super structure constituting the fimbrial adhesin.[30] The interplay between these two domains results in a dramatic change in FimH affinity to mannose and manossylated surfaces; when the pilin domain is disrupted, for example through a mutation rendering it structurally defective, the affinity of the lectin domain to mannose groups increases by up to three hundredfold.[31] The disruption of the pilin domain leads to increased mannose affinity and also mediates strong binding to surfaces even under low-shear conditions. The native FimH structure binds weakly under low-shear conditions, but strongly under high-shear conditions, which was attributed to a shear-induced mechanical separation of domains and thus switching the lectin domain from a low-to-high affinity state for binding.[5]

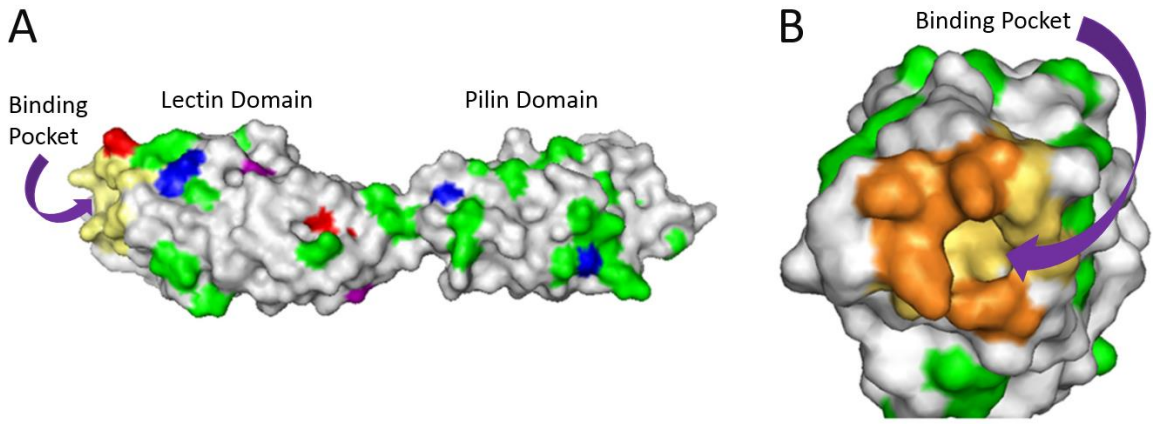

Figure 3: The fimbrial tip is composed of (A) two domain lectin and pilin protein containing (B) the mannose-binding pocket (yellow) at fimbrial tip responsible for attachment of fimbriae to surfaces.[32]

Studies of uropathogenic *E. coli* and *Klebsiella pneumoniae* FimH adhesins, both of which are 279 AAs in length, but vary by 15% in AA residues, revealed mutations in the lectin domain of FimH that resulted in higher binding affinity.[32] As seen in Figure 3, the two-domain structure of FimH contains a mannose-binding pocket in the lectin domain that is connected by a linker chain of 3 AAs to the pilin domain, incorporating the lectin domain into the fimbrial super unit. Regions in red represent mutations that increase mannose binding; yellow regions represent mutations where monomannose binding is increased; regions in orange represent mutations where polymannose binding is increased; and the region in light yellow showcases the mannose-binding pocket.

The lectin domain of the FimH adhesin also has implications in cellular hydrophobicity. The lectin family consists of carbohydrate-binding proteins that are often hydrophobic in nature.[33] Studies of the structure and binding thermodynamics of the fimbrial binding pocket showed that the binding of FimH to mannose α-D-mannopyranose results in a negative change in entropy, favoring the bound state of mannose to the lectin domain.[12] The polar FimH binding pocket is flanked on each side by Tyr48 and Tyr138 residues – which are hydrophobic AAs. As shown in Figure 4, these two AA residues form the "tyrosine gate" lining the FimH binding pocket which confers the hydrophobic properties observed in fimbriae.[34]

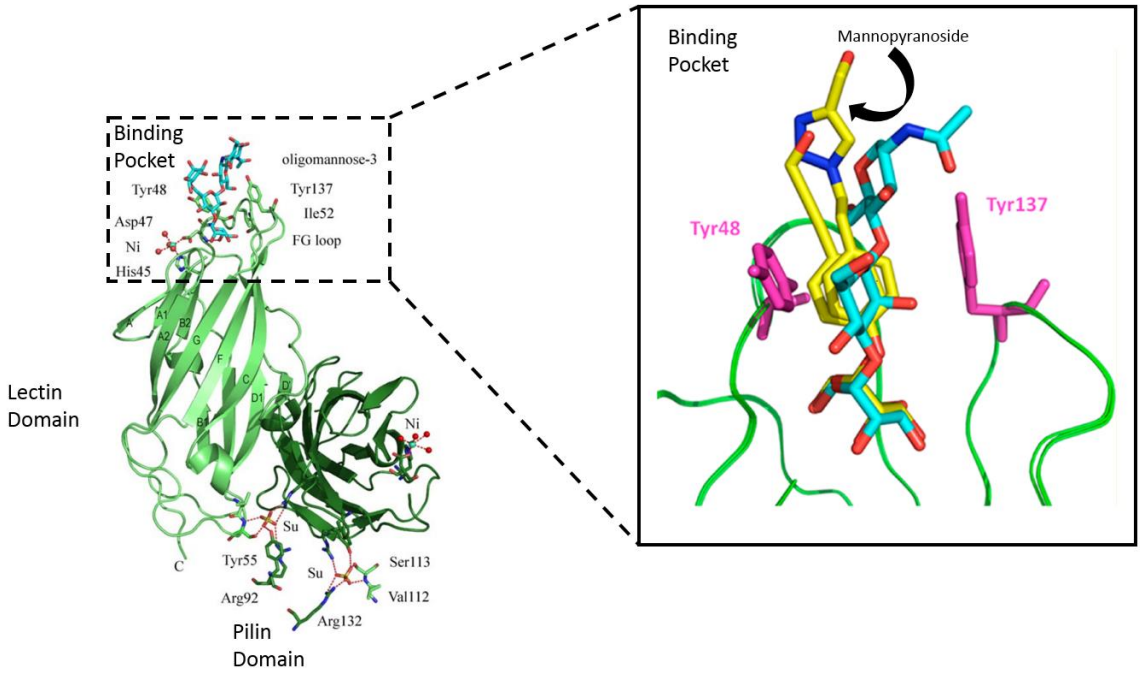

Figure 4: Hydrophobic "tyrosine gate" flanks the mannose binding pocket to mediate binding of mannose-containing groups to the FimH adhesin.[12,34,35]

The hydrophobicity of the FimH adhesin has direct implications for cellular adhesion to abiotic surfaces. The body of most bacterial species is negatively charged; based on Derjaguin, Landau, Verwey, and Overbeek (DLVO) theory, electrostatic repulsion should prevent cells from attaching to many negatively charged abiotic surfaces; nonetheless, cells are able to attach to abiotic surfaces despite the presence of a repulsive energetic barrier.[36] The presence of fimbriae around on the cell surface may promote cellular attachment, either by creating an extended soft polymer layer that reduces surface potentials below the energy barrier needed for cellular attachment to abiotic surfaces13 or by exploiting the smaller surface area of fimbriae to avoid [or reduce] electrostatic repulsion during cellular approach.[37] Cellular attachment to abiotic surfaces and subsequent biofilm formation is strongly correlated to the presence of fimbria on cells.[38] This ultimately suggests that while the FimH adhesin is specific to mannose and mannosylated surfaces (biotic), it also has the ability to attach to abiotic surfaces via on

non-specific binding from hydrophobic and electrostatic interactions. Furthermore, studies involving fimH deletions resulted in at least a three log reduction in colony forming units (CFUs) gathered from biofilms formed in silicon tubing.[39,40]

2.3 Remediation Techniques

Three general strategies exist for the treatment of contaminated environmental sites such as water and soil: biological, chemical, and physical treatment. Chemical and physical treatment of environmental contaminants have historically been the most common methods of remediation as they are more controlled, expedient, and time sensitive.[41] Nonetheless, bioremediation remains an established method for remediation of soils and groundwater, accounting for twelve percent of ex situ treatment projects and eleven percent of in situ treatment projects at Superfund sites across the US (Fig. 5).[42] Bioremediation techniques can be enhanced by adding rate-limiting nutrients to the microbial environment of the contaminated site or used in tandem with existing chemical or physical methods to provide a more economically viable route for environmental remediation.[18,42]

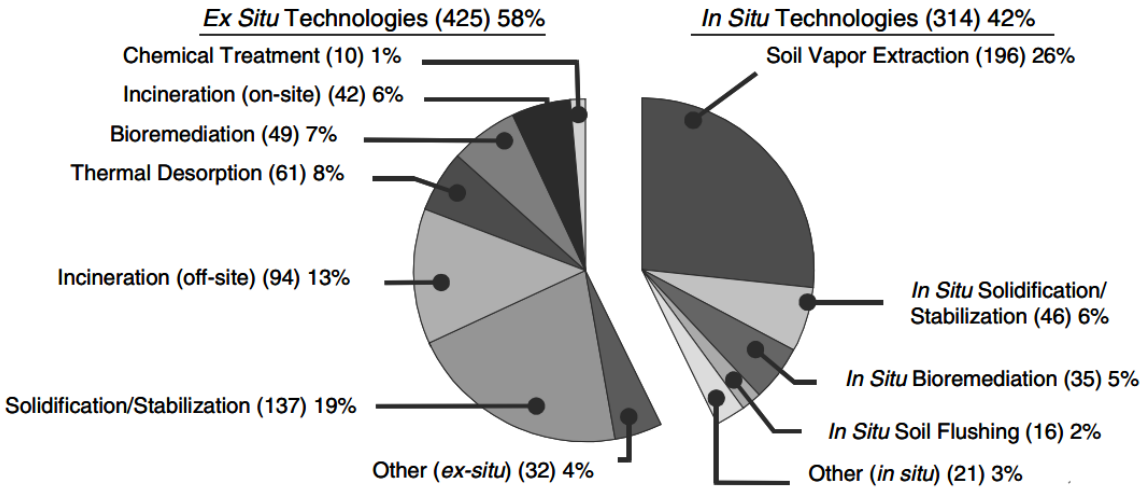

Figure 5 Superfund source treatment projects by category.[42]

Bioremediation treatments generally follow one of several different strategies. First, organic compounds can be degraded into carbon dioxide and water or methane (mineralization); one specific example is the degradation of benzene in water into CO_2 and methane.[43] Second, organic compounds can be transformed into smaller and less toxic or dangerous compounds; one example is the biotransformation of 2,4,6-trinitrotoluene (TNT), a toxic mutagen, into amino-substituted aromatics and toluene.[44,45] Third, electrophilic halogen and nitro groups on organic compounds can be biologically reduced; on example is the biodegradation of tetrachloroethene (PCE), a chlorocarbon, to ethane.46 Finally, heavy metals can be immobilized through a change in the valence state to a less toxic form; one example is the change of hexavalent chromium to trivalent.[47,41] Other biomediated heavy metal sequestration techniques have been used in the complexation of cadmium by phytochelatin (PC) and mercury by metallothionein (MT).[48,49] Commonly, bioremediation strategies are applied to organic (carbon-containing) compounds, to inorganic pollutants commonly found in fertilizers such as ammonia, nitrate, and perchlorates, and heavy metals. The vast majority of bioremediation sites deal with organic compounds, the most prominent of which being petroleum based hydrocarbons such as polycyclic aromatic hydrocarbons (PAHs) and BTEX (benzene, toluene, ethylbenzene, xylenes). These account for 40% and 37%, respectively, of contaminated sites. Furthermore, industrial wood preserving and hydrocarbon processing facilities account for over 50% of superfund sites where bioremediation is used as the primary method of cleanup.[42]

2.4 Engineered Species for Bioremediation

The massive use of petroleum products in developed countries has often led to contamination of the environment by release of hydrocarbon products and derivatives. One major such instance was the Deepwater Horizon (DWH) oil spill in the Gulf of Mexico in 2010 where $6.7x10^5$ metric tons of crude oil was released into the environment, believed to be the largest marine-based release of all time.[50] The DWH oil spill not only released the range of linear alkanes used in petrol, but it also released unspecified amounts of benzene, toluene, ethylbenzene, and xylenes (BTEX), polycyclic aromatic hydrocarbons (PAH), and many other others. BTEX and PAHs are also found widely in the industrialized areas that process petroleum-based chemicals and are of keen interest due to their higher water solubility and ability to contaminate groundwater and sediments.[51] BTEX and PAHs are listed as priority pollutants by the US EPA and are both toxic and carcinogenic; therefore, their removal from the environment is important and of keen interest to the scientific community.

One such method for the remediation of these hydrocarbons is the use of microbes for degradation and removal of such pollutants. Due to the well understood biochemical and genetic nature of *Escherichia coli*, many of the specific biodegrading genes found in other species have been heterologously combined for expression in *E. coli*. The combination of genes across species into *E. coli* has allowed us to better understand and even improve the functions of such genes.[52] For instance, pyrene, a polyaromatic hydrocarbon (PAH) consisting of four fused benzene rings, was shown to be degraded by a consortium (YL) of microbial species (mostly unidentified, but included Bacillus cereus); unknown plasmids from this consortium were then extracted and transformed into

competent *E. coli* cells. After transformation, the *E. coli* with YL plasmids was grown in the presence of PAHs and the degradation of PAHs was monitored via high performance liquid chromatography (HPLC) to show that various PAHs were degraded by *E. coli* transformed with unknown plasmids in the YL consortium.[53,54] In this case, the well understood characterization of *E. coli* allowed for the degradation of PAHs in a controlled manner from an unknown and uncontrollable source.

With the prominence of BTEX as pollutants in many industries, a great deal of research concerning the biodegradation of these compounds has been conducted. The metabolic break down of molecules into smaller units for energy or other anabolic reactions, or catabolism, of BTEX has been extensively studied via the *tod* and *tol* metabolic pathways (originating from *Pseudomonas putida* F1 and *Pseudomonas putida* mt-2).[55–59] However, the majority of research done on BTEX degradation has been on individual components therein, and not BTEX mixtures which are much more likely present in contaminated sites. When p-xylenes were degraded by the *tod* operon, a dead-end product (3,6-dimethylcatechol) was formed that could no longer be degraded.[60] In the TOL plasmid (pWW0), the enzyme xylene oxygenase cannot recognize and breakdown benzene as a substrate, thus preventing its degradation.[61] Furthermore, when two *P. putida* strains containing these pathways were combined, they did not result in full degradation of all BTEX. When separate plasmid parts were engineered and introduced in *E. coli*, the genes required for intermediate degradation products were elucidated. From this, researchers were able to introduce the genes involved in the complete mineralization of all BTEX components. When the cultures harboring the combination of genes in the *tod* operon and TOL plasmid were incubated in the presence of BTEX, UV-Vis, and HPLC

results showed no presence of metabolic intermediates (gas chromatography also showed no peaks outside of those associated with BTEX), unlike the simple combination of the two *P. putida* strains in a single culture.[62] This introduction of heterologous genes in *E. coli* has been extensively studied. Degradation of trichloroethylene (TCE) was successfully accomplished in *E. coli* by introduction of *todC1C2BA*, genes required for the enzyme toluene dioxygenase; not only did this confer *E. coli* with the ability to degrade TCE, but it also proved that only *todC1C2BA* was needed for this degradation pathway and not some unelucidated interaction between multiple genes or regulatory systems in the host organism.[63] Similar studies have been performed to study biphenyl, toluene, and benzene degradation in *E. coli* and the elucidation of genes required in the degradation thereof.[55,64,65]

Chapter 3 Experimental Methods

3.1 Plasmid Construction

Plasmids were designed in silico using SnapGene and the cloning history is given in the Supporting Information.

3.1.1 pPCC1401

Plasmid pPCC1401 was constructed by amplifying *fimA-H* from *Escherichia coli* MG1655 genomic DNA using primers pPCC1401-gib-for-NdeI and pPCC1401-gib-rev-XbaI, where the *E. coli* MG1655 genomic DNA was extracted using Qiagen's miniprep kit. Following this, polymerase chain reaction (PCR) was used to amplify and extract fimA-H from the genomic DNA using primers pPCC1401-gib-for-NdeI (pFG1-fimA-H_NdeI-for) and pPCC1401-gib-rev-XbaI (fim operon-XbaI-rev). The result of this PCR was ran on a gel to verify the length of the construct and then purified using Qiagen's gel cleanup kit. Following gel purification, a double digest of *fimA-H* was performed using the enzymes NdeI (5') and XbaI (3') and incubated at 37°C for 3 hours. The host vector pFG1 (AprR, pBR322 ORI) was also double digested using NdeI and XbaI. Once the double digests were gel purified, a ligation reaction with the cut and purified vector (pFG1/NdeI/XbaI) and insert (fimA-H/NdeI/XbaI) was performed using T4 ligase. Two reactions were ran: one with ONLY vector (pFG1) and one with vector AND insert (*fimA-H*). The resulting ligation reactions were then transformed into electrocompetent *E. coli* MC1061 cells and incubated overnight on Luria Bertani (LB)+Apramycin culture plates. The plates were checked in the morning for colonies; the plate with only the vector did not grow while the plate with the vector and insert had many colonies. Five separate colonies were selected from the V+I plate and cultured for a miniprep in the morning. The

minipreps were then ran on a gel to verify proper plasmid size/length. After verification of plasmid size, primers were designed for sequencing. Sequencing results were verified by GeneWiz.

3.1.2 pPCC1403

Plasmid pPCC1403 was constructed by linearizing host vector plasmid pFG28A (AprR, pBR322 ORI) using restriction enzyme digestion by HindIII (5') and SacII (3'). The cut vector fragment was then purified using Qiagen's gel extraction kit. The gene fragment *fimA-H* was amplified from plasmid pPCC1401 using the primers pPCC1403-gib-for-HindIII and pPCC1403-gib-rev-SacII. Gibson Assembly was then used to insert *fimA-H* into the cut pFG28A vector/host plasmid (HindIII and SacII) to create the new plasmid pPCC1403. Following linearization and purification, Gibson Assembly was performed to insert *fimA-H* into the cut pFG28A vector by using primers pPCC1403-gib-for-HindIII and pPCC1403-gib-rev-SacII. Plasmid pPCC1403 was constructed by excising the *His-egfp* gene from pFG28A by cutting with SacII and HindII and then using Gibson Assembly using primers to insert *fimA-H* into the cut vector.

3.1.3 Plasmid History

Plasmid pFG1 contains apramycin resistance and the pBR322 origin of replication as well as the lacI regulatory genes including the *lac* operator, *lac* promoter (inducible by IPTG), *lacI*, and the *tac* promoter (binds the lac repressor [LacI] to inhibit transcription; repression is relieved by addition of Isopropyl β-D-1-thiogalactopyranoside (IPTG) - the higher the concentration of IPTG, the higher the expression from P_{tac}). pFG1 also contained the *araC* regulatory gene, which was removed via double restriction digestion described earlier. The plasmid vector backbone of pPCC1403 (pFG28A) was based off of

the pFG1 plasmid; it contains the lacI/P_{tac} regulatory scheme that regulates a downstream GOI (*alkS*) which subsequently regulates P_{alkB} to control transcription of the *His-egfp* fluorescence tag (AprR, pBR322 ORI). The *His-egfp* gene was replaced by *fimA-H* using restriction digest of vector pFG28A, PCR amplification of *fimA-H*, and Gibson Assembly of the two gene fragments.

3.2 Yeast Agglutination Assay/Sedimentation Assay (YAA)

A modified yeast agglutination assay (YAA) was performed to semi-quantitatively measure the degree of fimbriation (DOF) of the engineered cells. Two methods were used to prepare yeast cultures, both of which resulted in the same level of detection of fimbriation. In the first method, industrial yeast pellets (Saccharomyces cerevisiae) were mixed in phosphate buffer solution (PBS) at a concentration of 5 mg/mL. In the second method, yeast pellets were grown overnight in Luria Bertani (LB) (37°C with shaking) and then centrifuged and washed with PBS twice. Following growth, the yeast suspension was then diluted to an optical density (OD) of 8.0 (OD595 on NOVOstar plate reader) in preparation for the assay.

Bacterial strains were grown from an overnight subculture starting at an OD of 0.05 and grown statically in LB +/- Apramycin, where specified, to an OD of 0.7; then, all cultures were induced with varying concentrations of IPTG and then grown until the late exponential phase. (NOTE: it is hard to grow these *E. coli* past an OD of 2 – 2.5 in static growth conditions). Next, the bacterial cultures were centrifuged and resuspended in PBS twice and diluted to an OD of 1.0 in preparation for the assay. After *E. coli* and yeast cells were grown, washed, and diluted, 500 μL of each suspension (yeast and bacteria) was transferred into a single centrifuge tube and the yeast and bacteria cells were allowed to

interact. Where noted, 100 mM D-mannose or methyl α-D-Mannopyranoside was added to bacterial suspensions 5 minutes before addition of yeast suspension to ensure full occupation of the FimH mannose-binding fimbrial tips.

After mixing of yeast and bacteria suspensions, the cells were allowed to react for 3, 6, 16, or 36 hours without agitation. Bacteria bound to yeast cells sedimented out of solution and deposited on the bottom of the centrifuge tubes; the opacity of the remaining solution depended on the reaction time. Then, each centrifuge tube was vortexed at ~2200 rpm (Analog Vortex Mixer, 120V, FisherScientific) for 10 seconds; solution turbidity was measured for each sample at 0, 3, 5, 10, 20, and 30 minutes after vortexing. For turbidity measurements, a 20 μL aliquot was removed from the tube; great care was taken to ensure that the aliquot was taken from the center of the centrifuge tube at the same depth for each measurement. The removed aliquot was diluted 10 times in PBS and turbidity/absorbance (595 nm wavelength) was measured in a 96-well plate. Each experiment was repeated at least three times.

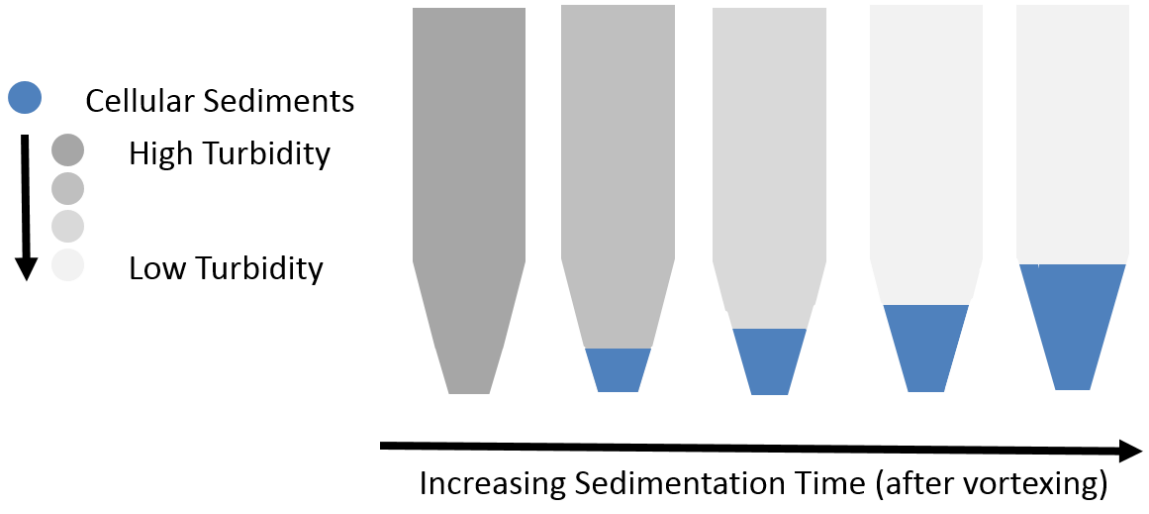

Figure 6: Yeast Agglutination and Sedimentation Assay

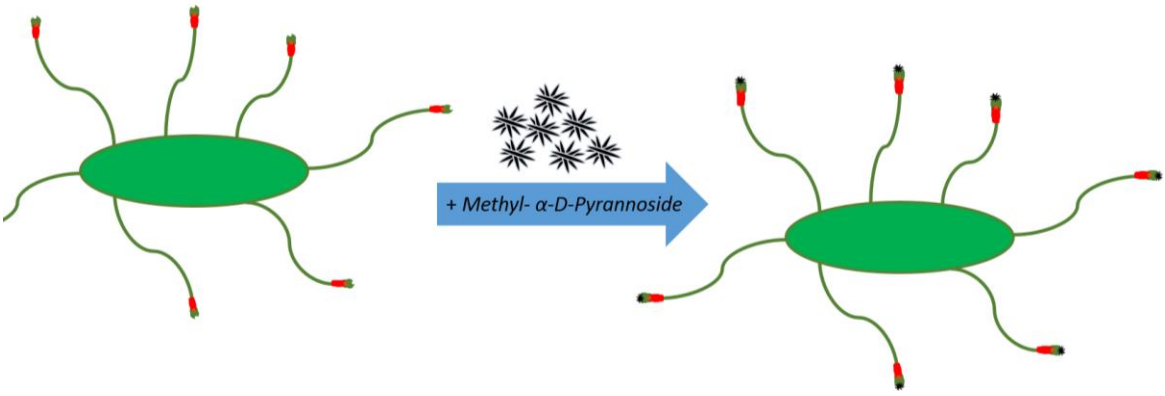

Figure 7: Surface Coverage of Fimbrial Adhesive Tips (FimH) by Methyl-α-D-Pyrannoside.

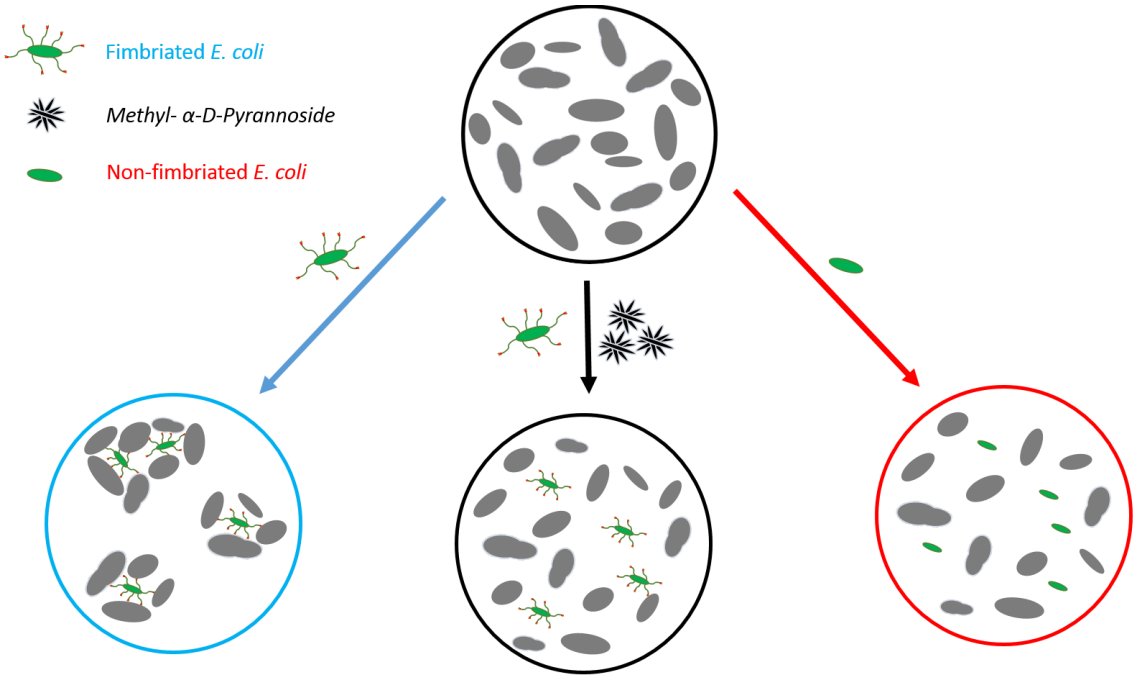

Figure 8: Methyl-α-D-Pyrannoside Mechanism of Inhibition for the Agglutination of Yeast Cells.

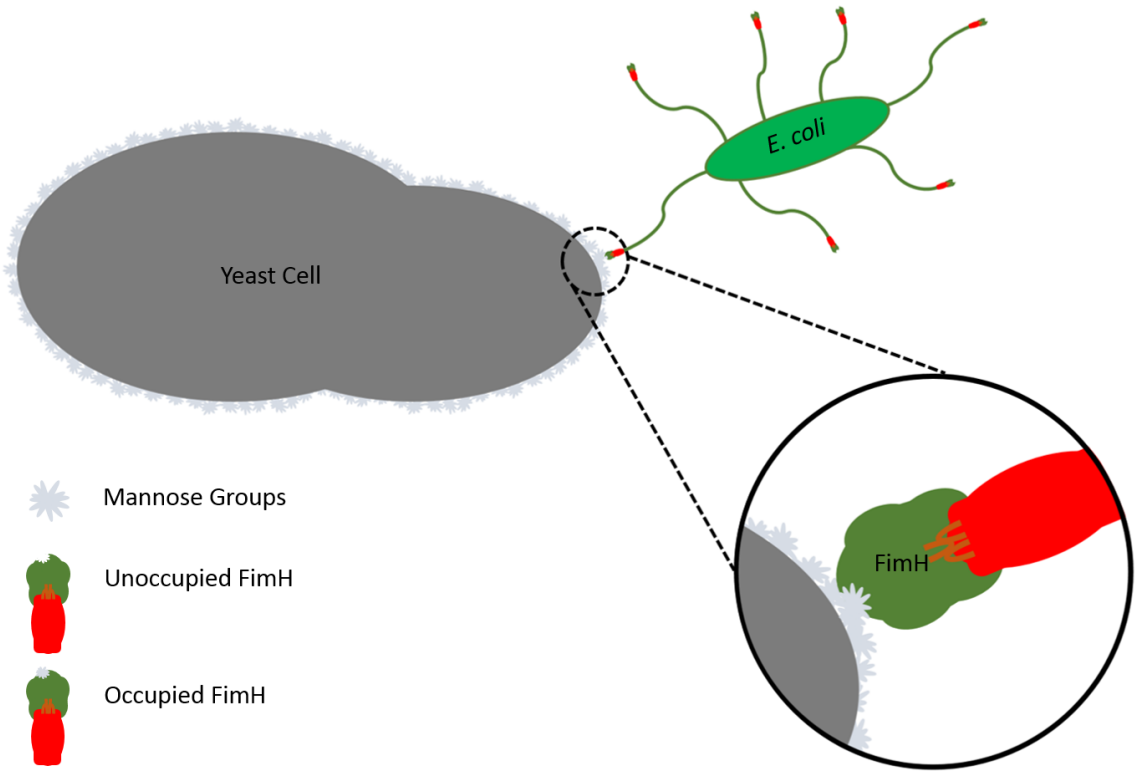

Figure 9: The FimH adhesin is responsible for binding of E. coli to yeast cells.

3.3 Microbial Adhesion to Hydrocarbons (MATH) Assay

A MATH assay was used to measure the cell surface hydrophobicity. In this assay, the absorbance of an aqueous cell suspension and a hydrophobic phase are measured before and after mixing to determine the concentration of cells that partition into the hydrophobic phase. Briefly, bacterial suspensions were allowed to grow to a desired OD and then centrifuged and washed in PBS twice to remove all carbon sources and thus stop or greatly hinder cell growth. Suspensions were then diluted to an OD of 1.0 in preparation for the MATH assay. After dilution, 4 mL of the cell suspension and 1 mL of a hydrocarbon liquid (n-dodecane, hexadecane, hexane, toluene/naphthalene mixture) were sequentially transferred into a 15 mL centrifuge tube. Each solution, containing cells and hydrocarbons, was vigorously vortexed at ~3200 rpm (Analog Vortex Mixer, 120V, FisherScientific) for

60 seconds and then allowed to rest and phase separate into two distinct liquid phases for 10 minutes (30 minutes if noisy readings). After phase separation, the OD of the bottom aqueous layer was measured with care to avoid carrying additional hydrocarbon into the 96-well plate. Each measurement was repeated at least three times. We report two metrics, the MATH(%)/Hydrophilicity defined as,

$$Hydrophilicity\ (\%) = \frac{OD_{595}\ Before\ Vortexing}{OD_{595} After\ Vortexing}\ x\ 100 \qquad (3.1)$$

and the fraction partitioned (Fp) into hydrocarbon phase defined as,

$$F_p = 1 - Hydrophilicity(\%) \quad (3.2)$$

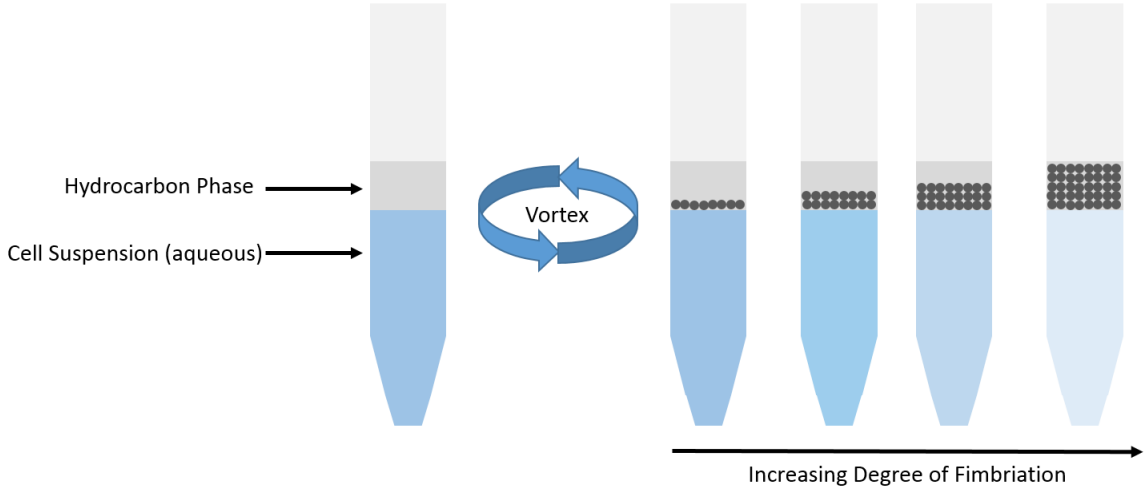

Figure 10: Microbial Adhesion to Hydrocarbon (MATH) Assay.

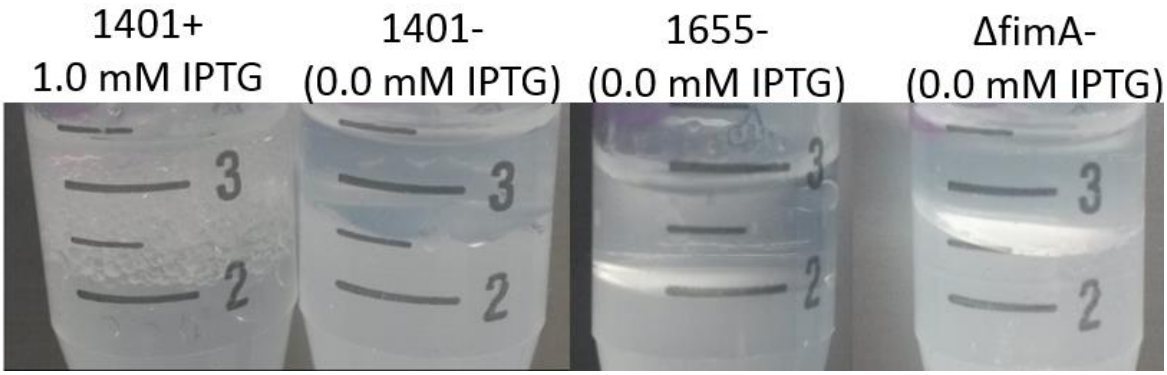

Figure 11: Visualization of MATH assay with increasing level of partitioning to hydrocarbon phase with increasing level of fimbrial expression.

3.4 Specific Biofilm Formation (SBF) Assay

The growth of bacterial biofilm formation over time was quantified via the growth of bacterial cultures in sterile 96-well plates. Cell cultures were grown overnight from a fresh colony and subcultured the following morning (starting at OD 0.05) and allowed to grow to mid-exponential phase. This suspension was then diluted to an OD of 0.2 immediately prior to the start of the biofilm assay. 300 µL aliquots of the cell culture were injected into wells of a sterile 96-well plate, which was then covered with sterile aluminum foil; the 96-well plate and aluminum covers were sterilized via soaking in ethanol for one hour under UV radiation source. The 96-well plate was then quiescently incubated at 30°C for 12, 24, or 48 hours. Following incubation, aliquots of liquid cultures were diluted 10:1 in LB media and the OD of the diluted liquid cultures were measured (to quantify relative cell growth). The remaining cell solutions were decanted/removed from the wells. Each well was then washed three times in 300 µL of PBS to remove unbound cells followed by well staining in 300 µL of 0.1% crystal violet (CV) in DI water (50 µg in 50 mL H2O) for 20 minutes. After incubation, the CV stain was removed and the wells were again washed three times in PBS; the biofilm was subsequently eluted via addition of 300 µL of an

acetone/ethanol mixture (20:80, v/v) to solubilize the bound cells from the surface of the wells66. The OD of the eluted CV-stained biofilm was then measured to quantify the level of biofilm development by each cell type. Each assay was repeated for twelve replicates from two separate cultures. These values were then averaged to calculate the specific biofilm formation (SBF)67 of each cell type

$$SBF = \frac{(B - NC)}{G} x\ 100, \tag{3.3}$$

where B is the amount of CV-stained biofilm formed, NC is the amount of CV adhered to the 96-well plates due to abiotic factors (i.e., a measure of film formation in LB without cells), and G is the optical density of cells grown in each suspended culture.

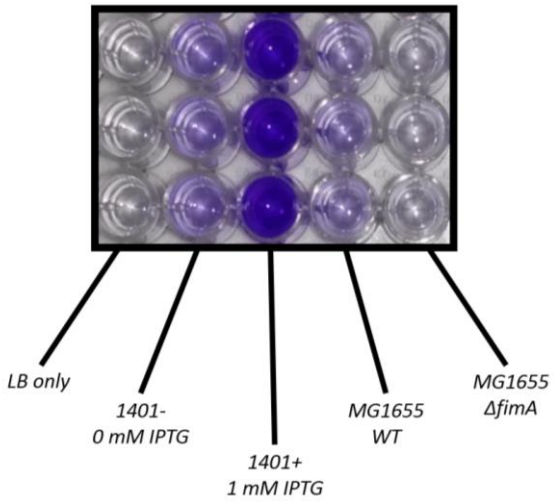

Figure 12: Biofilm formation increases with increasing level of fimbriation. From left to right (periphery wells left blank): LB only, 1401- (0.0 mM IPTG + glucose), 1401+ 1.0 mM IPTG, MG1655, MG1655ΔfimA.

3.5 Transmission Electron Microscopy (TEM) Imaging

Type I fimbriae are 4 – 10 nm in width and 0.5 - 2.1 μm in length and are too small to be resolved with conventional light microscopy. Instead, TEM imaging was used to visually confirm the presence or absence of fimbriae. To image cell surface appendages,

cultures were grown one of two ways: from an overnight subculture in LB or from a culture that was cleaned and resuspended in HEPES buffer (fixed in 0.1% glutaraldehyde solution). One day prior to imaging, cells were grown overnight from a subculture and grown to the late exponential phase, then cleaned and resuspended in 10 mM HEPES buffer. Later in the evening (the night before imaging, ~12 hours) the washed cells were resuspended in a 0.1% glutaraldehyde solution to fix the cells. The second method of cell processing for TEM imaging was accomplished by growing cells in standard LB (from a subculture) with induction of fimbriation by addition of 1.0 mM IPTG and diluted to an OD of 0.5 the morning of imaging (essentially, no processing). There was no significant difference in quality of images obtained for these methods of cell preparation.

After cell preparation, and prior to grid incubation, two 20 uL drops of DI water and two 20 uL drops of uranyl acetate were deposited onto a piece of Parafilm (manufacturer). Next, 2 – 5 µL of a bacterial suspension were pipetted onto a freshly glow-discharged carbon-coated TEM grid and allowed to sit for 30 – 90 seconds. Following this incubation period, the cell-adsorbed grid was twice quickly washed in water: the grid was transported by forceps into a small 20 µL drop of DI water on wax paper (~1 second) and dried by touching its outer edge with a chemwipe to wick away excess water. After washing, the grid was quickly deposited into the 20 uL drop of 2% (w/v) uranyl acetate (~1 second) and then blotted dry with a chemwipe; uranyl acetate staining was repeated, except this time, the sample was allowed to stain for 15 seconds and then wicked dry. The grids were then allowed to air dry. Prepared grid specimens were then loaded into the TEM holder, inserted into the stage, and pumped down to the stage pressure. Samples were observed in a JEOL 1200 EX TEM operated at an acceleration voltage of 100kV and

electron micrographs were recorded using a 2k slow-scan CCD camera (model 14C, SIA) at a user-defined magnification. Areas in the sample with uneven stain or positive staining with a large amount of black contrast were avoided, whereas cells with lighter staining were sought out.

Chapter 4 Manipulation of fim Operon for Fimbrial Expression in *Escherichia coli*

4.1 Methodology

4.1.1 Materials

The *Escherichia coli* strains used in the study of manipulation and control of fimbrial expression were MG1655-WT, MC1061-WT, MG1655ΔfimA, MG1655ΔfimA-pPCC1401, and MG1655ΔfimA-pFG1. The yeast agglutination assay used the industrial baker's yeast Saccharomyces cerevisiae. Common growth and preparation media used for bacterial strains and for yeast were Luria Bertani (LB) broth (5 g yeast extract, 5 g NaCl, 10 g Bacto-tryptone in 1 L total volume H2O, procured from BD Chemical); LB agar (5 g yeast extract, 5 g NaCl, 10 g Bacto-tryptone, and 15 g agar procured in 1 L total volume H2O, from BD Chemicals); phosphate buffer solution (PBS) (8 g NaCl, 0.2 g KCl, 1.44 g Na2HPO4, 0.24 g KH2PO4 dissolved in 800 mL of H2O and pH adjusted to 7.4 [with HCl] followed by the addition of H2O to 1 L); and apramycin sulfate (antibiotic, 50 µg/mL in distilled H2O, sterile filtered, from Carbosynth).

4.1.2 Preparation

All *E. coli* and yeast cells were grown statically from an overnight starter culture inoculated from a single colony on LB-agar plates at 37°C +/- antibiotics, where specified. From this, subcultures were prepared by diluting cells from the overnight cultures into a desired volume of LB-broth with a starting optical density (OD) of 0.05 and grown until an OD of 0.7 was reached (~2.5-3 hrs); at this OD (0.7), 1mM IPTG was added where indicated and grown for 16 hours without shaking (late exponential phase), unless otherwise noted. Following growth, cells were processed by centrifuging at 4000g for 15 minutes to pellet the cells and then decanting the LB solution, the pellet was then

resuspended in an equal volume of PBS and then centrifuged again at 4000g for 15 minutes and decanted, this PBS wash was repeated again and the cell pellet was resuspended in half the starting volume of PBS. Following this final wash, cells were prepared for assaying by diluting the solutions to an OD of 1.0, except where indicated.

4.2 Assays and Characterization

4.2.1 Yeast Agglutination and Sedimentation Assay (YAA)

The experimental preparation and measurement procedure for the yeast agglutination and sedimentation assay (YAA) was described in Section 3.2. All data were obtained using a NOVOstar plate reader (BMG Labtech) operating at a wavelength of 595 nm to measure the optical density of a solution containing bacteria and yeast cells. We report the average and standard deviation of the absorbance over n = 6 replicates. The yeast agglutination assay measures the change in the absorbance in solution as fimbriated bacterial strains attach to and agglutinate yeast cells, forming larger clusters that sediment out of solution. The rate at which aggregates sediment out of solution provides a relative metric of the level of fimbriation of the bacteria: the higher the level of fimbriation, the faster the rate of sedimentation and the more rapidly the absorbance of the solution decreases. The settling velocity (V_s) of a particle with a Reynold's number less than 0.1 (Stokes' Law) is

$$V_s = \frac{g(\rho_p - \rho)D_p^2}{18\mu}, \tag{4.1}$$

where g is gravitational acceleration, ρ_p is the density of the settling particles (1.087 g/mL), ρ is the density of the medium in which the particles are suspended (0.998 g/mL), D_p^2 is the diameter of the settling particles, and μ is the viscosity of the fluid medium (1.0 cP).

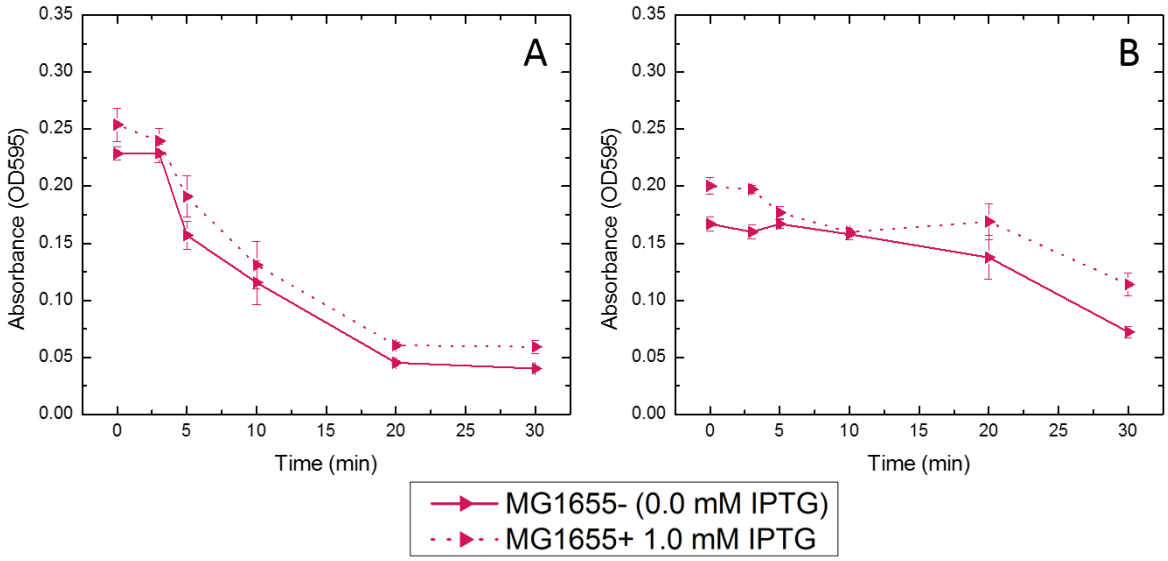

Figure 13: Yeast agglutination assay (YAA), measuring absorbance as a function of time for E. coli strain MG1655 with and without addition of IPTG for mixing times of (A) 3 hours and (B) 36 hours. IPTG addition did not result in any increase in sedimentation rate.

To determine whether the addition of the inducer IPTG affected the ability of bacteria to express fimbriae and thus agglutinate yeast, we first performed a YAA on the wild-type bacteria strain, MG1655, in the presence and absence of IPTG. The yeast agglutination assay (YAA) was carried out after two different *E. coli*/yeast reaction/interaction times: 3 and 36 hours. At each reaction time point, the presence and/or absence of IPTG for each mixing time showed similar sedimentation rates, independent of IPTG (Fig. 13). The opacity of the MG1655 cell suspension decreased by a factor of two to three over thirty minutes. The decrease in the turbidity seen in the above figure for MG1655 suggests that there exists some amount of naturally expressed fimbria in the wild-type strain.

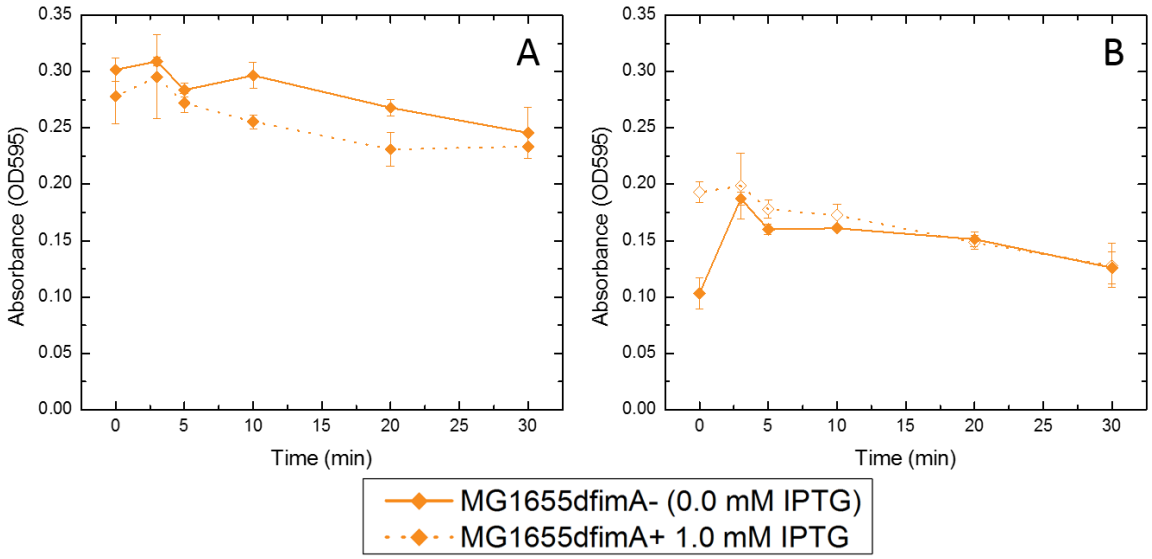

Figure 14: Yeast agglutination assay (YAA), measuring absorbance as a function of time for E. coli strain MG1655ΔfimA with and without addition of IPTG for mixing times of (A) 3 hours and (B) 36 hours. IPTG addition did not result in an increased sedimentation rate.

Similarly, the effect of IPTG on fimbriation was tested for the fimbriae-deletion strain MG1655ΔfimA. Over thirty minutes, the opacity of the solution remained relatively constant for three hour reaction (Figure 14A) and addition of IPTG did not change the ability of cells to agglutinate yeast. Similarly, for a 36 hour reaction the addition of IPTG did not have an effect on the agglutination of yeast cells (Fig. 14B), although the absorbance of both solution decreased somewhat. The relatively slow sedimentation rate seen in MG1655ΔfimA over a thirty minute period indicates the absence of fimbria in this strain.

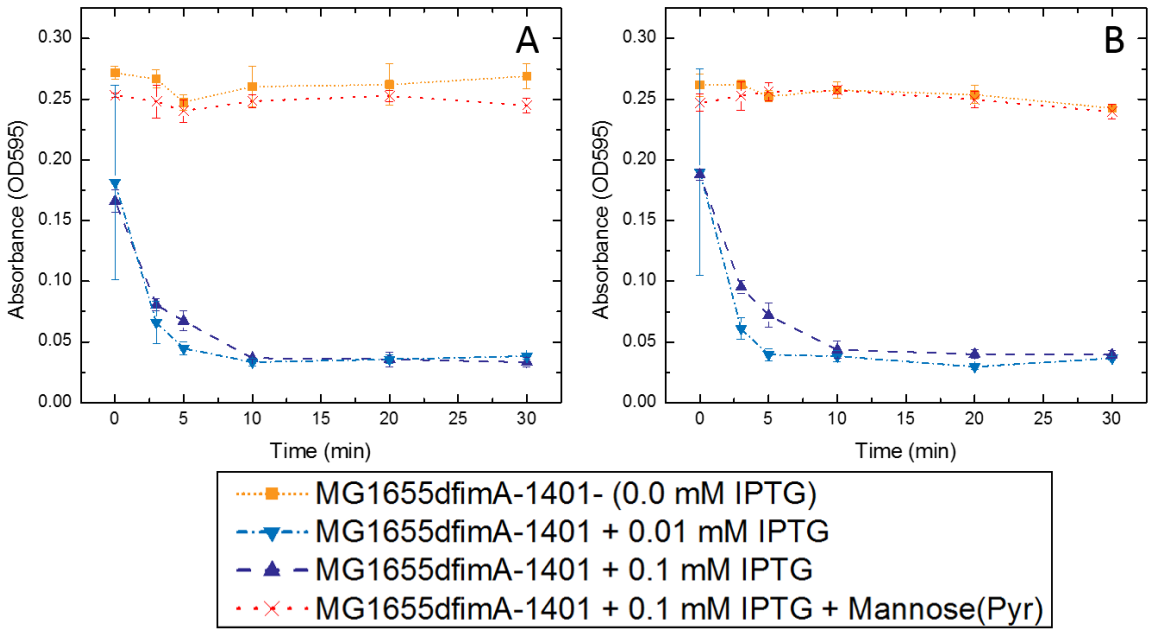

Figure 15: Yeast agglutination assay (YAA), measuring absorbance as a function of time for E. coli strain MG1655ΔfimA-pPCC1401 with and without addition of IPTG for mixing times of (A) 3 hours and (B) 36 hours. The addition of IPTG resulted in a dramatic increase in the rate of sedimentation.

The bacterial strain engineered to express fimbriae upon induction, MG1655ΔfimA-pPCC1401, showed marked differently sedimentation behavior in the YAA depending on the presence or absence of the inducer IPTG. Upon adding IPTG at concentrations of 10 to 100 μM, the absorbance decreased faster for the MG1655ΔfimA-pPCC1401 strain than for than non-induced MG1655ΔfimA-pPCC1401 at all reaction time points (Fig. 15). This rapid decrease in turbidity indicates agglutination of yeast cells, suggesting the presence of fimbriae. To confirm that the binding of bacterial fimbriae to yeast cells generated the faster change in absorbance, we added methyl-α-D-pyrranoside (Mann(pyr), which is chemically similar to mannose) to an induced strain of MG1655ΔfimA-pPCC1401. The addition of Mann(pyr) resulted in a sedimentation response similar to the uninduced MG1655ΔfimA-pPCC1401 strain; this result suggested that when mannose was present, the FimH adhesin became occupied and no longer capable

of mediating cellular attachment. In all cases, the presence of IPTG caused MG1655ΔfimA-pPCC1401 to agglutinate and sediment out yeast cells at a much higher rate than the controls across all reaction times.

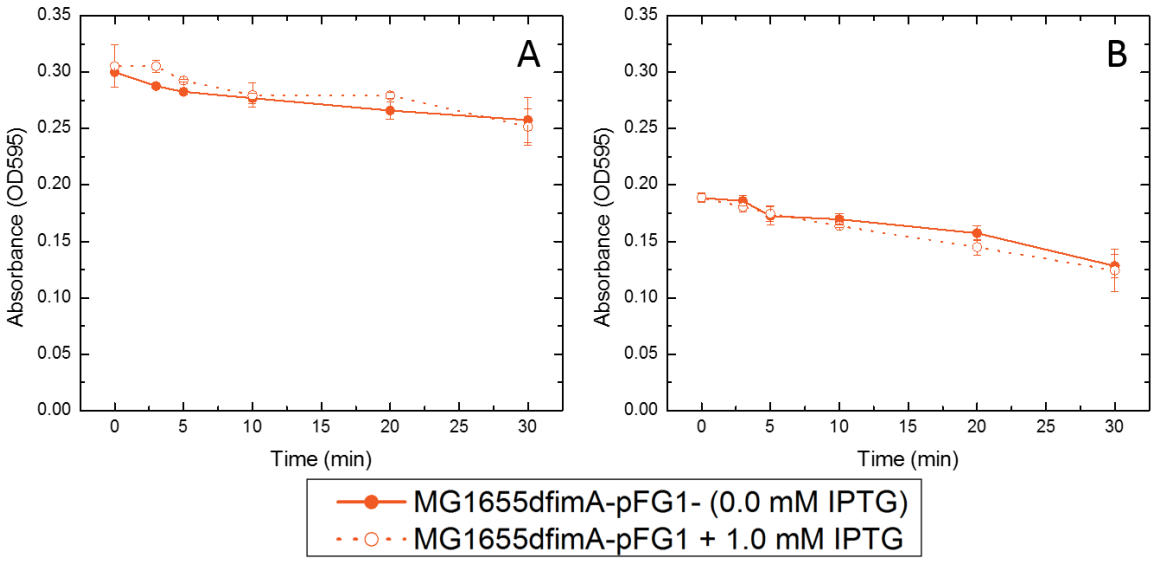

Figure 16: Yeast agglutination assay (YAA), measuring absorbance as a function of time for E. coli strain MG1655ΔfimA-pFG1 with and without addition of IPTG for mixing times of (A) 3 hours and (B) 36 hours. IPTG addition did not result in any increase in the sedimentation rate.

The parent plasmid of pPCC1401 was pFG1. A YAA was carried out using MG1655ΔfimA-pFG1 to see if the unique agglutinating power of pPCC1401 was a remnant of the parent plasmid vector pFG1. The ability of MG1655ΔfimA-pFG1 to agglutinate yeast does not change with and without the presence of the inducer IPTG. Additionally, the opacity of the cell suspension remained relatively constant across most time points, suggesting that MG1655ΔfimA-pFG1 played no role in the agglutination of yeast cells.

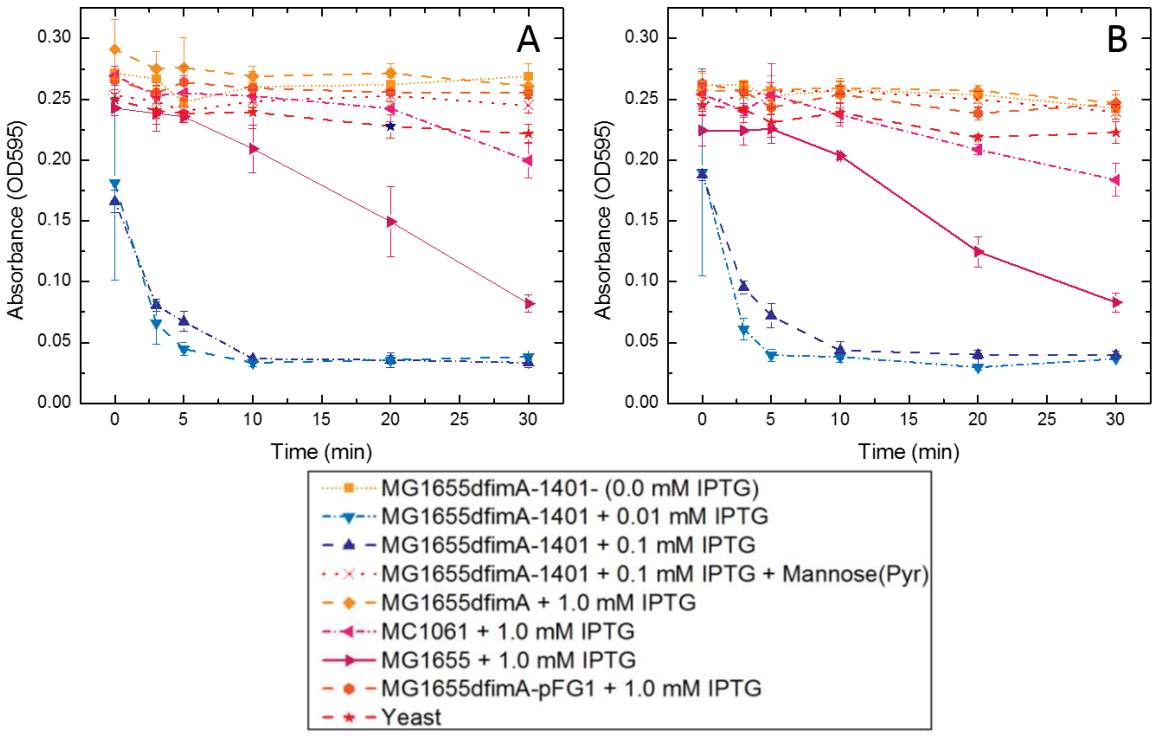

Figure 17: Yeast agglutination assay (YAA), measuring absorbance as a function of time for all E. coli strain tested with and without addition of IPTG for mixing times of (A) 3 hours and (B) 36 hours. The addition of IPTG in MG1655ΔfimA-pPCC1401 resulted in a dramatic increase in the rate of sedimentation, while wild-type MG1655 displayed a moderate sedimentation rate.

To assess the relative extent of fimbriation in all strains, we compared the results of the YAA across all strains and all additives. Induction of MG1655ΔfimA-pPCC1401 by 10 or 100 μM IPTG resulted in a significantly increased sedimentation rate of cellular suspensions (Fig. 17). The rapid decrease in absorbance in the first five minutes of the assay indicated that cells rapidly sedimented out of suspension; after this time, the absorbance reached a plateau of 0.05. The agglutinating power of wild-type MG1655 was relatively intermittent between the engineered strains and the remaining control strains – as seen by the purple line in between the two major trends. The remaining experiments [1401- (0.0 mM IPTG), 1401+ 0.1 mM IPTG + Mann(Pyr), dfimA + 1.0 mM IPTG, MC1061 + 1.0 mM IPTG, pFG1 + 1.0 mM IPTG, and yeast] showed little sedimentation over the thirty-minute time-course of the assay; the absence of a pronounced response in

the initial sedimentation rates of these unfimbriated control strains suggests that fimbriae are essential for the attachment and agglutination of yeast cells by *E. coli*.

4.2.2 Microbial Adhesion to Hydrocarbon Assay (MATH)

After the cells were grown and processed, the samples were processed as described in Section 3.3 in preparation for the microbial adhesion to hydrocarbon (MATH) assay. Following the assay, the average and standard deviation of n = 6 optical density measurements were compared across difference hydrocarbons and bacterial strains. Three alkanes of varying chain length were tested in the MATH assays: hexane (C6), dodecane (C12), and hexadecane (C16); the dielectric constants of these alkanes were 1.88, 2.01, and 2.08, respectively. In addition, the aromatic hydrocarbon toluene (dielectric constant 2.38) was also tested for in the MATH assays.

The tendency of the cells in solution to partition themselves into the hydrocarbon phase was quantified using Equations 3.1 and 3.2 in Section 3.2.3. The percent hydrophilicity (Eq. 3.1), corresponding to the fraction of cells remaining in aqueous solution, was calculated from opacity measurements in the aqueous phase; the corresponding fraction partitioned into the hydrocarbon phase was derived from this metric. Higher values of percent hydrophilicity indicated that cells were more likely to remain in the aqueous phase. The fraction partitioned (F_p) represents the fraction of cells that left the aqueous phase and moved into the hydrocarbon phase, and was calculated using Equation 3.2 in the Experimental Methods chapter.

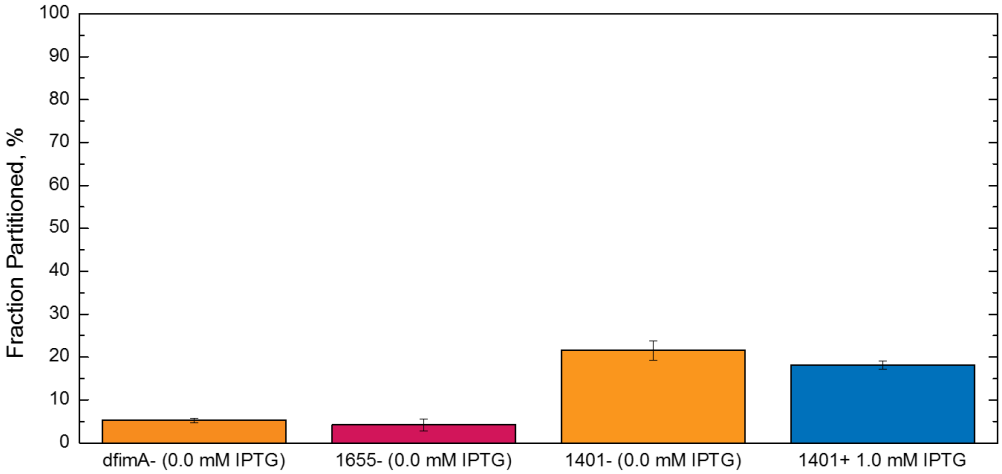

Figure 18: Microbial Adhesion to Hydrocarbon (MATH) Assay in hexane, measuring absorbance as a function of microbial hydrophobicity in ΔfimA, MG1655, pPCC1401 without induction, pPCC1401 with induction. Engineered strain MG1655ΔfimA-pPCC1401 partitioned into the hydrocarbon phase at the highest rate.

The adhesion of cells to the hydrocarbon hexane was also measured. Most cells showed little partitioning into hexane, as shown in figure 4.6. Both 1401- 0.0 mM IPTG and 1401+ 1.0 mM IPTG resulted in similar levels of partitioning, with values of 21 and 18, respectively; the standard deviation of 1401- 0.0 mM IPTG was double that of 1401+ 1.0 mM IPTG suggesting the leaky expression of fimbriae in uninduced 1401. The wild-type strain MG1655- 0.0 mM IPTG and the fimbrial deletion strain ΔfimA- 0.0 mM IPTG resulted in the same levels of partitioning, with F_p of 4 and 5%, respectively. The fraction of partitioned cells was always higher in the strains with the engineered plasmid pPCC1401 than in those without (Fig. 18), suggesting the presence of fimbriae – which contain hydrophobic tyrosine groups at the FimH tip. Such hydrophobic moieties may explain the increased level of partitioning of 1401 into hexane.

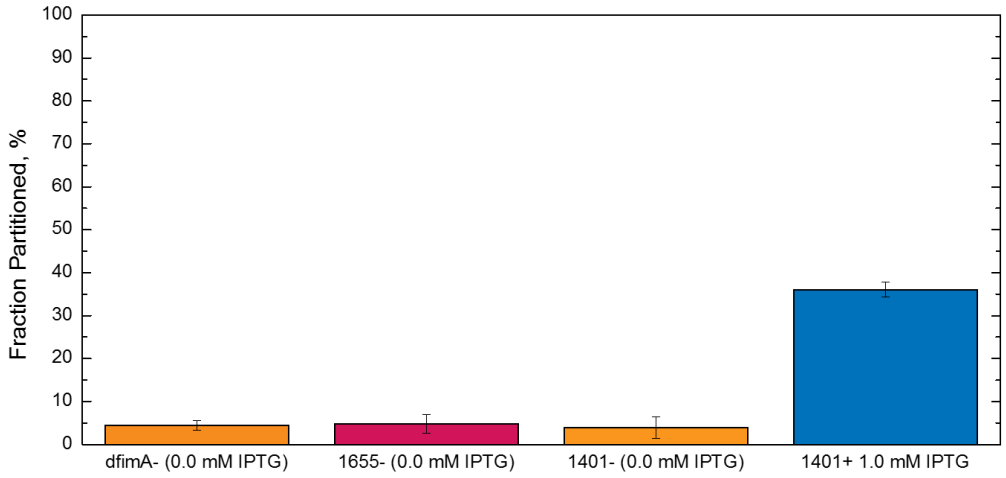

Figure 19: Microbial Adhesion to Hydrocarbon (MATH) Assay in dodecane, measuring absorbance as a function of microbial hydrophobicity in ΔfimA, MG1655, pPCC1401 without induction, MG1655ΔfimA-pPCC1401 with induction. Engineered strain MG1655ΔfimA-pPCC1401 partitioned into the hydrocarbon phase at the highest rate.

To determine the effect of alkane chain length on the tendency of bacterial strains to partition into hydrocarbons, we also performed MATH assays using dodecane (Figure 19) and hexadecane (Figure 20). The tendency of bacterial strains to partition into dodecane was measured. Cells of the induced strain, 1401+ 1.0 mM IPTG, were significantly more likely to partition into the hydrocarbon phase, with partitioned fraction of 37%, compared to all other strains (Fig. 19). The remaining strains showed relatively the same level of partitioning with values of 4%, 5%, and 4.5% for 1401- 0.0 mM IPTG, MG1655- 0.0 mM IPTG, ΔfimA- 0.0 mM IPTG, respectively. The same trends observed for dodecane were also observed for hexadecane (Fig. 20). The induced strain, 1401+ 1.0 mM IPTG, showed an increased level of hydrophobicity compared to the other strains, with nearly 70% of cells partitioning into the hydrocarbon. The partitioned fractions of cells into the hydrocarbon phase for 1401- 0.0 mM IPTG, MG1655- 0.0 mM IPTG, ΔfimA- 0.0 mM IPTG were essentially the same (2%) with standard deviations larger than the values measured themselves (Fig. 20).

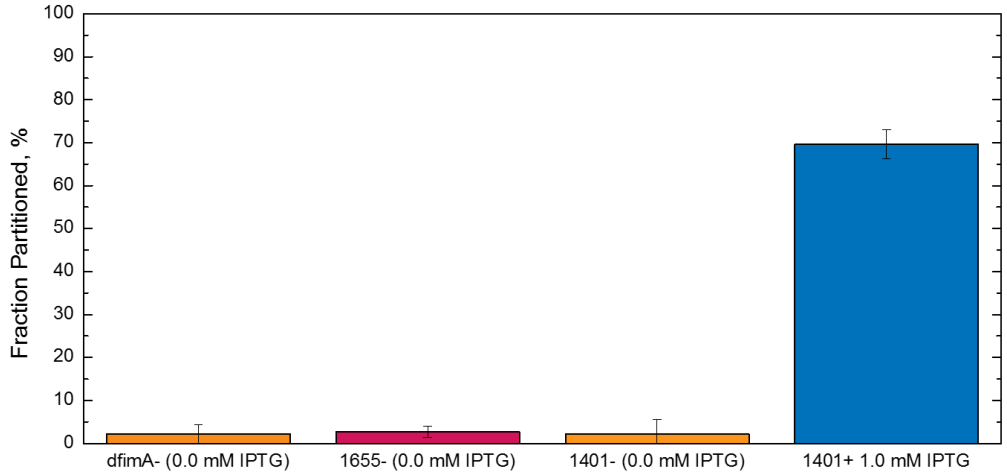

Figure 20: Microbial Adhesion to Hydrocarbon (MATH) Assay in hexadecane, measuring absorbance as a function of microbial hydrophobicity in ΔfimA, MG1655, pPCC1401 without induction, pPCC1401 with induction. Engineered strain MG1655ΔfimA-pPCC1401 partitioned into the hydrocarbon phase at the highest rate.

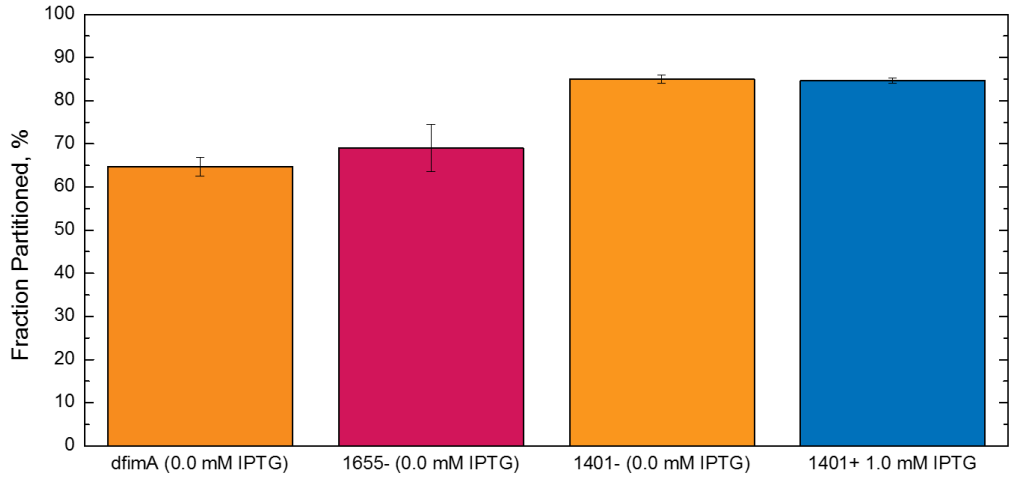

Figure 21: Microbial Adhesion to Hydrocarbon (MATH) Assay in toluene, measuring absorbance as a function of microbial hydrophobicity in ΔfimA, MG1655, pPCC1401 without induction, pPCC1401 with induction. Engineered strain MG1655ΔfimA-pPCC1401 partitioned into the hydrocarbon phase at the highest rate.

Both the induced (1401- 0.0 mM IPTG) and uninduced (1401+ 1.0 mM IPTG) bacterial strains carrying the plasmid pPCC1401 for over fimbriation resulted in approximately the same level of partitioning into the hydrocarbon phase (F_p = 83%), as shown in Figure 21. Wild-type bacteria (MG1655- 0.0 mM IPTG) and bacteria with a fimbrial deletion (ΔfimA- 0.0 mM IPTG) were slightly less likely to partition, with

corresponding F_p values of 69% and 65%, respectively. The error on MG1655 wild-type was significantly larger than any of the other strains; this may have been a result of different native expression levels of fimbria across the separate cultures used in the MATH assays. The level of partitioning of cells into the hydrocarbon phase was relatively high for all strains, compared to the three other hydrocarbons tested.

4.2.3 Specific Biofilm Formation (SBF)

Samples for quantification of biofilm formation were prepared as described in Section 3.4 of Materials and Methods. All samples were grown statically at 37°C. The average and standard deviation of absorbance of n = 12 biofilm samples were acquired for each SBF assay at three time points: 12, 24, and 48 hours. The specific biofilm formation (SBF) was calculated from the measurements of cell growth and biofilm growth using Equation 2.3 in Section 2.2.4. Biofilm development was quantified via a plate reader operating at a wavelength of 595 nm. Biofilm absorbance measured the total level of biofilm formation without regards to relative cellular growth rates of each strain. The specific biofilm formation was standardized to abiotic control wells that contained only the LB growth medium. Higher values of SBF indicated higher rates of biofilm growth (relative to cell growth rate).

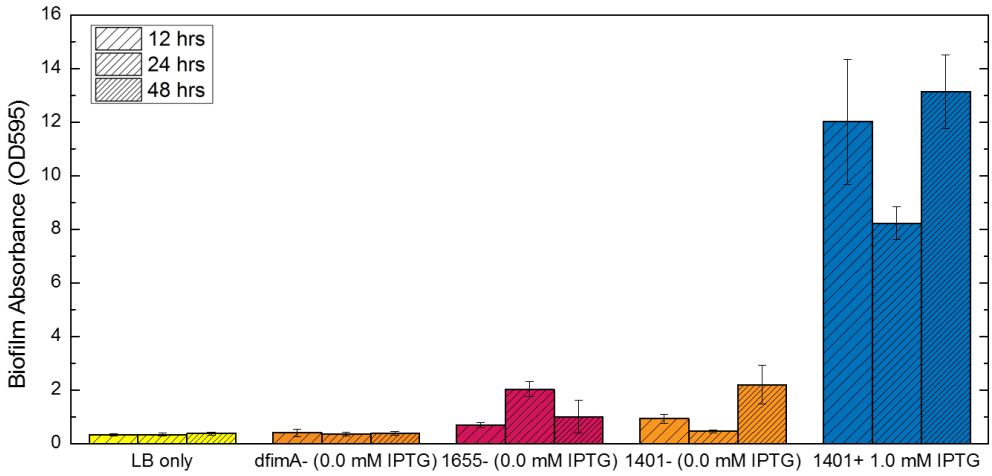

Figure 22: 96-well plate biofilm formation assay, measuring the absorbance of crystal violet (CV) stained biofilms as a function of time. For each sample, biofilm absorbance was measured at 12 h (sparsely shaded), 24 h (medium shading), and 48 h (dense shading). The engineered strain MG1655ΔfimA-pPCC1401 developed the highest amount of biofilm.

The absorbance of biofilm-containing solutions, reported in Figure 22 without correcting for the rate of cellular growth, varied with strain and inducer concentration. The biofilm formation for each strain did not exhibit consistent trends with time, as shown in Figure 22. The induced and fimbriated strain 1401+ 1.0 mM IPTG exhibit the highest absorbance and hence the highest biofilm formation. By contrast, little biofilm formation was observed in the uninduced strain 1401- 0.0 mM IPTG and the wild-type strain MG1655- 0.0 mM IPTG. The lowest biofilm formation was observed for the fimbrial deletion strain ΔfimA- 0.0 mM IPTG; the absorbance of these samples was statistically indistinguishable from that of the control wells of LB growth media only (without cells). The highest level of biofilm formation was observed in 1401+ 1.0 mM IPTG, while all other strains produced a substantially smaller amount of biofilm, suggesting that 1401 expressed a significantly higher degree of fimbriation.

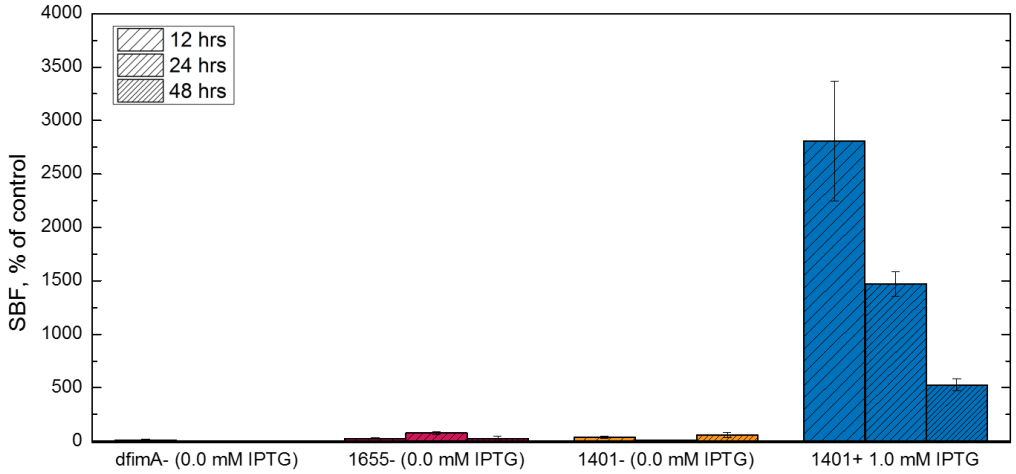

Figure 23: Specific Biofilm Formation (SBF) assay, measuring the absorbance of crystal violet stained biofilms as a function of time and semi-normalized to bacterial growth. For each sample, SBF absorbance was measured at 12 h (sparsely shaded), 24 h (medium shading), and 48 h (dense shading). The engineered strain MG1655ΔfimA-pPCC1401 developed a much higher SBF than all controls.

The specific biofilm formation also quantifies the total biofilm formation, but corrects for non-specific staining due to abiotic factors (i.e., residual stain in control wells with only LB) and normalizing the total biofilm absorbance value by the relative growth of each sample. The induced fimbriated stain, 1401+ 1.0 mM IPTG, generated the highest level of biofilm formation, as quantified by SBF in Figure 23, with the greatest levels of specific biofilm formation (relative to cellular growth) occurring at the earliest time point. Lower SBF was observed for the uninduced strain (1401- 0.0 mM IPTG) and the wild-type strain (MG1655- 0.0 mM IPTG); the standard deviations across n = 6 measurements were large compared to the value of the SBF. The strain with the fimbrial deletion (ΔfimA- 0.0 mM IPTG) showed almost no biofilm formation; furthermore, the standard deviations for the fimbrial deletion strain were 2-3 times larger than the value of the SBF. Similar to the trend seen in figure 23, the specific biofilm forming ability of the strain engineered for fimbrial expression showed the highest level of biofilm formation – with 1-2 orders of

magnitude higher biofilm development than all other strains; such results indicate that the presence of fimbriae is essential in initial biofilm formation.

4.2.4 Transmission Electron Microscopy (TEM) Imaging

Cells were prepared for transmission electron microscopy (TEM) imaging using the procedure described in Section 3.5. Samples were then imaged in a JEOL 1200 EX TEM at a user-defined magnification to confirm the presence or absence of fimbriae.

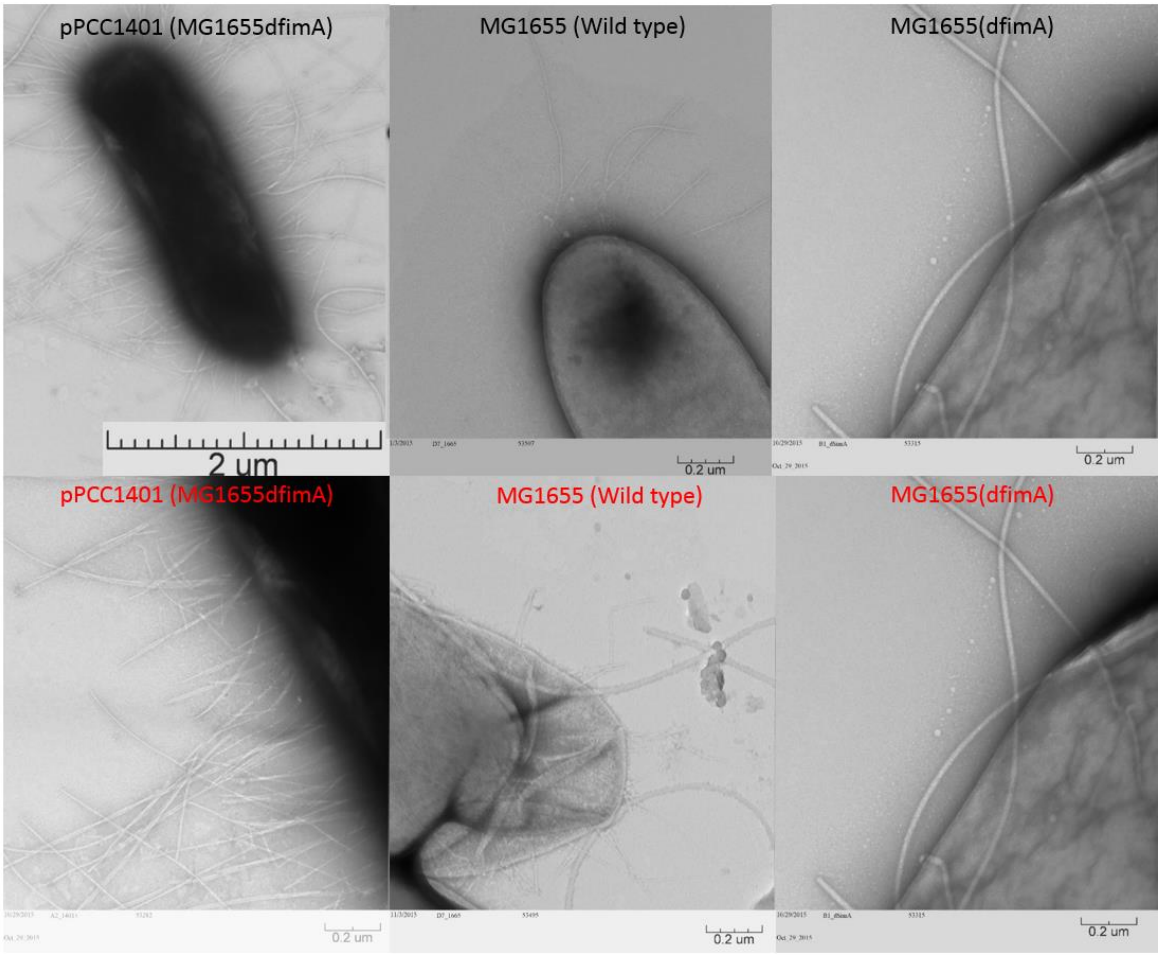

Figure 24: Transmission electron micrographs of induced MG1655ΔfimA-pPCC1401 (left, engineered strain), MG1655 (center, wild-type), and MG1655ΔfimA (right, fimbrial deletion). The engineered strain MG1655ΔfimA-pPCC1401 displayed many more fimbriae than wild-type MG1655, while MG1655ΔfimA displayed no fimbriae.

The presence of fimbriae in the engineered bacteria strain with plasmid pPCC1401 is readily seen in TEM imaging, as shown in Figure 24. The presence of fimbriae on the

wild-type strain (MG1655) can be vaguely seen. By contrast, the strain with a fimbrial deletion (MG1655ΔfimA) showed no presence of fimbriae in the TEM images. At a higher magnification, the presence of individual fimbriae on the engineered strain (MG1655ΔfimA-pPCC1401) was much more pronounced than in the wild-type strain (MG1655). There was no presence of fimbriae on the strain with a fimbrial gene deletion (MG1655ΔfimA). Such images validate the presence of fimbriae in the engineered strain (MG1655ΔfimA-pPCC1401) and substantiate the results of previous assays.

4.3 Discussion

To elucidate the effect of cellular fimbriation on biofilm development and binding affinity to select surfaces and biologically relevant molecules, the plasmid pPCC1401 was engineered to overexpress fimbrial development on the outer membrane of a fimbrial-deletion mutant of *E. coli* strain MG1655. The degree of fimbriation of the engineered MG1655ΔfimA-pPCC1401 strain was compared to that of wild-type MG1655, which expresses a native level of fimbriation; to MG1655ΔfimA-pFG1, which contains the parent vector of pPCC1401 expressing the apramycin antibiotic selection marker and promoter sequence involved in IPTG induction; and to MG1655ΔfimA, which lacks the major fimbrial subunit protein FimA required for structural development of viable fimbriae. The presence or absence of fimbriae on each strain was determined using a variety of experimental methods, including the yeast agglutination and sedimentation assay (YAA), microbial adhesion to hydrocarbon assay (MATH), specific biofilm assay (SBF), and transmission electron microscopy (TEM) imaging.

The ability of *E. coli* expressing fimbriae to agglutinate yeast and red blood cells is well documented in the microbiology and medical literature.[68–71] To determine the extent

to which the presence of fimbriae were able to agglutinate yeast, a modified yeast agglutination and sedimentation assay (YAA) was developed; in this assay, the relative degree of fimbriation expressed by each strain was related to the rate of sedimentation of cells in solutions containing *E. coli* and yeast. As the number of fimbriae on each cells increases, the agglutination of yeast and *E. coli* cells is expected to increase. The increase in aggregate diameter leads to an increase in the rate of sedimentation, which scales with the effective aggregate diameter squared (Eq. 4.1). The sedimentation rate of the induced engineered strain MG1655ΔfimA-pPCC1401 was significantly higher than the non-induced sample (Fig. 15). As the concentration of inducer (IPTG) increased, the sedimentation rate of the solution increased slightly but was not significant within experimental errors. Nonetheless, the sedimentation rate of MG1655ΔfimA-pPCC1401 (at any level of IPTG induction) was significantly higher than that measured for any strain lacking fimbriae. Similarly, when methyl-α-D-pyrranoside (a non-metabolizable analogue of mannose) is present during the reaction, the FimH binding domain of fimbriae binds to Mann(Pyr); the fimbriae are unable to bind the yeast cells and so the rate of sedimentation in this mixture is comparable to that in non-fimbriated and uninduced strains. Outside of the engineered and induced strains, only the wild-type MG1655 strain showed any significant level of fimbriation. The rate of sedimentation observed for MG1655 was between that of the non-fimbriated strains and the strains engineered for increased degree of fimbriation, suggesting an intermediate degree of fimbriation (Fig. 17). The observed trend of increasing sedimentation rate with increased degree of fimbriation supports the agglutination trends in an earlier study, which reported an increase in aggregate size with strains of *E. coli* containing higher degrees of fimbriation.[72]

A well-established method to characterize the level of cellular hydrophobicity is the microbial adhesion to hydrocarbon (MATH) assay.[73–76] The MATH assay quantifies the fraction of cells that partition into a hydrophobic hydrocarbon phase through the change in optical density of the aqueous cellular solution before and after agitation. As discussed in Section 2.2, the FimH adhesin is a two-domain system, in which a pilin domain connects a lectin domain to the major fimbrial subunit (FimA) with a mannose-binding "pocket" located at the lectin tip; this binding pocket is lined with hydrophobic tyrosine AA residues. Therefore, bacterial cells expressing a larger number of fimbriae should result in a higher fraction of cells that partition into a hydrophobic hydrocarbon phase, F_p. Indeed, the strain engineered for fimbriation (MG1655ΔfimA-pPCC1401) exhibited the highest value of F_p over all strains for all four hydrocarbons tested (hexane, dodecane, hexadecane, and toluene). The highest values of F_p were observed for aromatic toluene, for all strains, however, MG1655ΔfimA-pPCC1401 showed a significantly higher partitioning than did the wild-type MG1655 and MG1655ΔfimA. Similar MATH results in toluene were reported for a "hydrophobic" bacterial strain.[73] For the smallest alkane chain tested (n-hexane), approximately twenty percent of the fimbriated strain MG1655ΔfimA-pPCC1401 partitioned into the hydrocarbon phase, whereas a negligible fraction of cells in MG1655 and MG1655ΔfimA partitioned. A greater fraction of cells partitioning into the longer chain alkanes, n-dodecane and n-hexadecane, with F_p of forty and seventy percent, respectively. These results are consistent with those reported in an earlier study of *E. coli* in n-dodecane.[15]

Type 1 fimbriae have been shown to greatly enhance biofilm formation on both biotic and abiotic surfaces.[29,14,77] To quantify the extent of biofilm formation by various

bacterial strains, biofilms grown in 96 well plates are stained with crystal violet and then extracted with various ethanol mixtures.[57–60] Here, we found that the highest total biofilm formation for any time point was achieved in the strain engineered for fimbrial overexpression, MG1655ΔfimA-pPCC1401, which was at least five times higher than any other sample. The total amount of biofilm formed by wild-type MG1655, which expressed fimbriae, was higher than the fimbrial deletion strain MG1655ΔfimA and on par with the amount of biofilm formed via leaky expression of the non-induced MG1655ΔfimA-pPCC1401. Biofilm formation was almost non-existent in MG1655ΔfimA, and was not statistically distinguishable from biofilm formation due to residual residues from the LB control wells without cells. Together, these results indicate the presence of fimbriae is essential for initial biofilm formation to occur. Absolute biofilm formation, however, is a poor measurement because it does not account for differences in cellular growth rates or for non-specific CV staining of the control wells. The specific biofilm formation (SBF) calculated in Equation 3.3 takes into account these factors;[67] this normalized metric of biofilm formation more accurately quantifies biofilm formation with respect to the presence of fimbriae. After normalization, the effect of fimbriae expression on *E. coli* biofilm forming ability was far more pronounced, with MG1655ΔfimA-pPCC1401 displaying at least an order of magnitude more biofilm forming ability than any of the controls (Fig. 23).

The relative abundance of fimbriae on the surface of the strains used in these assays was verified through direct imaging with transmission electron microscopy (Fig. 24). The fimbrial deletion mutant MG1655ΔfimA showed absolutely no fimbrial on the cellular membrane and the wild-type MG1655 showed few fimbriae. By contrast, the engineered

strain, MG1655ΔfimA-pPCC1401, showed a significantly increased presence of fimbriae on the cell's outer-membrane.

4.4 Conclusion

In this chapter, *E. coli* was genetically engineered to over-express fimbriae under control of the P_{tac} promoter, allowing the expression of fimbriae to be inducible by the lactose-mimicking and non-metabolizable inducer molecule IPTG. The plasmid pPCC1401 was designed to contain all genes necessary for fimbrial development and inducible expression. This plasmid was transformed into MG1655ΔfimA to produce MG1655ΔfimA-pPCC1401. Several assays were performed to compare the relative degree of fimbriation of this engineered strain to various controls, including wild-type MG1655, MC1061, MG1655ΔfimA, MG1655-pFG1, and non-induced MG1655ΔfimA-pPCC1401. The agglutinates of yeast and the engineered bacterial strain MG1655ΔfimA-pPCC1401 sedimented out of suspension more rapidly than any of the controls tested. Furthermore, a greater fraction of MG1655ΔfimA-pPCC1401 cells partitioned into the hydrocarbon phase than in any of the controls. These results confirmed that the engineered strain controllably expressed fimbriae. The presence of fimbriae in the engineered strain (and absence in the controls) was confirmed through TEM imaging, which revealed that the engineered strain, MG1655ΔfimA-pPCC1401, expressed more fimbriae than any of the controls. Finally, the presence of fimbriae on *E. coli* increased the biofilm forming ability of the engineered and induced strain MG1655ΔfimA-pPCC1401 by at least an order of magnitude. The presence of fimbriae assists in the attachment of bacterial cells to substrates, promotes hydrophobicity, and stimulates biofilm formation which may be utilized to attach to and colonize areas of hydrocarbon contamination.

Chapter 5 Alkane-Inducible Fimbriation for Bioremediation Processes

5.1 Methodology

5.1.1 Materials

The *Escherichia coli* strains used in the study of manipulation and control of fimbrial expression were MG1655-WT, MC1061-WT, MG1655ΔfimA, MG1655ΔfimA-pPCC1401, MG1655ΔfimA-pFG1, MG1655ΔfimA-pFG28A, and MG1655ΔfimA-pPCC1403. The yeast agglutination assay used the industrial baker's yeast Saccharomyces cerevisiae. Common growth and preparation media used for bacterial strains and for yeast were Luria Bertani (LB) broth (5 g yeast extract, 5 g NaCl, 10 g Bacto-tryptone in 1 L total volume H2O, procured from BD Chemical); LB agar (5 g yeast extract, 5 g NaCl, 10 g Bacto-tryptone, and 15 g agar procured in 1 L total volume H2O, from BD Chemicals); phosphate buffer solution (PBS) (8 g NaCl, 0.2 g KCl, 1.44 g Na2HPO4, 0.24 g KH2PO4 dissolved in 800 mL of H2O and pH adjusted to 7.4 [with HCl] followed by the addition of H2O to 1 L); and apramycin sulfate (antibiotic, 50 µg/mL in distilled H2O, sterile filtered, from Carbosynth).

5.1.2 Preparation

Yeast and bacterial cells were grown statically from an overnight starter culture inoculated from a single colony on LB-agar plates at 37°C +/- antibiotics (where specified). From this culture, subcultures were prepared by diluting cells from the overnight cultures into a desired volume of LB-broth with a starting optical density (OD) of 0.05 and grown until an OD of 0.7 was reached (~2.5 – 3 hrs). Once the culture reached this OD, IPTG was added at various concentrations (0.01 mM to 5 mM) and grown for 16 additional hours without shaking. Following growth, cells were centrifuged at 4000g for 15 minutes to

generate a pellet and the LB solution was decanted. Subsequently the pellet was twice resuspended in an equal volume of PBS and then centrifuged again at 4000g for 15 minutes. After the washes, the cell pellet was resuspended in half the initial volume of PBS. Following this final wash, cells were prepared for assays by diluting the solutions to an OD of 1.0, except where indicated.

5.2 Assays and Characterization

5.2.1 Yeast Agglutination and Sedimentation Assay (YAA)

A detailed description of the YAA experiments is provided in Section 3.2. Briefly, planktonic *E. coli* cells of a known concentration were mixed with yeast cells of a known concentration and allowed to mix for a set amount of time (3 or 36 hours). After agitation, aliquots of this cellular suspension were taken across time at a constant height (1.1 centimeters) in the reaction vessel. The more fimbriae present on the outside of *E. coli* cells, the more yeast cells will agglutinate; the more cells that agglutinate, the larger the diameter of the cell particle [or cluster] and the faster that cells will fall out of solution. Hence the rate of sedimentation (through the decrease in absorbance of the solution) provides a measure of the extent of fimbriation of the bacteria. Similar to the study presented in Chapter 4, the goal of this chapter is to controllably induce fimbriation in the presence of a model inducer molecule, dicyclopropyl ketone (DCPK), which activates transcription of the genes necessary for fimbriation. The goal of the YAA experiments is to assess the extent of fimbriation in response to exposure to DCPK. The plasmid MG1655ΔfimA-pPCC1403 contains a dual-inducible regulatory system that allows for the expression of the gene *alkS*, which we placed under the control of the IPTG inducible P_{tac} promoter. The protein AlkS acts as a transcriptional regulator and is able to bind to smaller

chain alkanes (C5-C12) and to the model inducer DCPK to activate the P_{alkB} promoter and the subsequent transcription of genes downstream of the promoter.

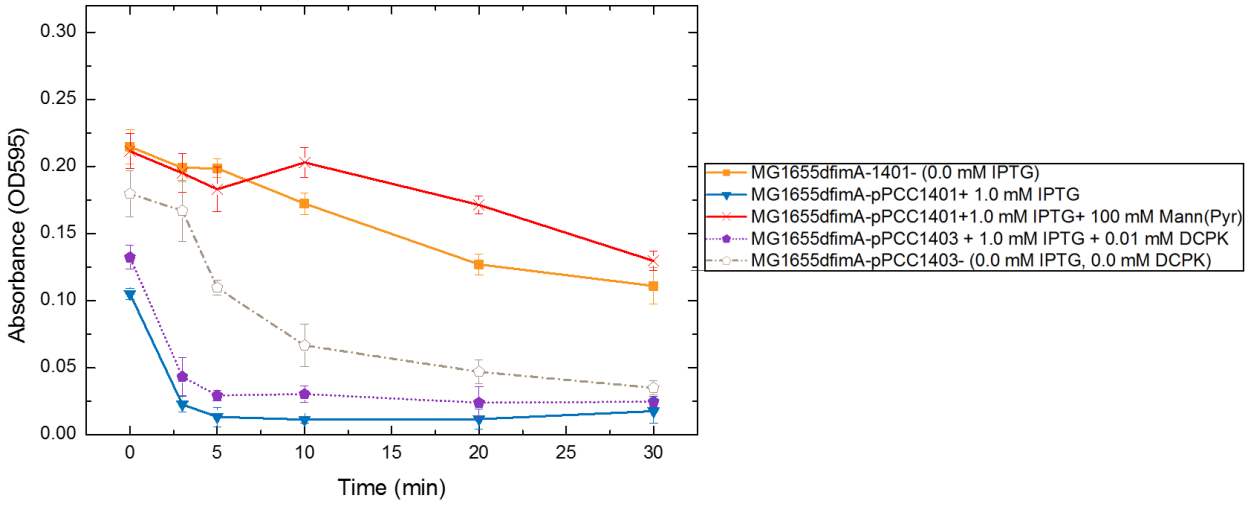

Figure 25: Yeast agglutination assay (YAA), measuring absorbance as a function of time for MG1655ΔfimA-pPCC1401 and dual-inducible expression of fimbriae in MG1655ΔfimA-pPCC1403. The presence of inducers IPTG and DCPK played a large role in the sedimentation rate.

The agglutinating strength of the alkane-inducible MG1655ΔfimA-pPCC1403 strain for a single concentration of DCPK and IPTG was comparable to the agglutinating abilities of the IPTG inducible MG1655ΔfimA-pPCC1401 strain, as seen in Figure 25. The alkane-inducible strain (MG1655ΔfimA-pPCC1403, shown with dotted lines) with or without inducers is compared to the IPTG inducible strain (MG1655ΔfimA-pPCC1401); a filled marker indicates presence of inducers (IPTG and DCPK) and an unfilled marker indicates the absence of the aforementioned inducers. The uninduced MG1655ΔfimA-pPCC1403 strain showed a relatively high level of expression, even with the addition of glucose to prevent the leakiness of the IPTG inducible system. MG1655ΔfimA-pPCC1401 without inducer showed a much more controllable expression level and a similar level of agglutination compared to MG1655ΔfimA-pPCC1401 assay allowed to bind/interact to methyl-α-D-pyrannoside.

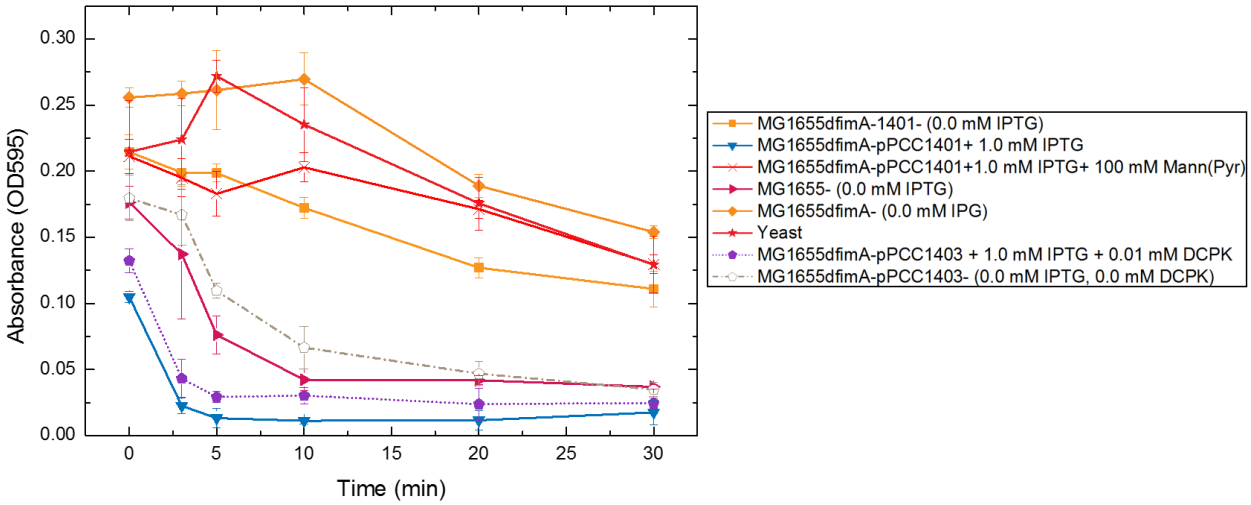

Figure 26: Yeast agglutination assay (YAA), measuring absorbance as a function of time for dual-inducible MG1655ΔfimA-pPCC1403 compared to IPTG-inducible MG1655ΔfimA-pPCC1401 and controls. MG1655ΔfimA-pPCC1403 showed the same sedimentation rate as MG1655ΔfimA-pPCC1401.

The relative agglutination rates of induced MG1655ΔfimA-pPCC1401 and induced MG1655ΔfimA-pPCC1403 were similar, as shown in Figure 26. The cellular suspensions including these strains sedimented within the first five minutes and exhibited a significantly lower level of turbidity compared to the controls of MG1655ΔfimA-pPCC1401 without induction, MG1655ΔfimA-pPCC1401 with methyl-α-D-pyrannoside, plain yeast suspension, and MG1655ΔfimA. The level of sedimentation of the wild-type MG1655 strain was intermediate to between that of the two engineered strains and that of the controls; most aggregates formed by MG1655 sedimented out of solution after ten minutes and the turbidity of the solution after thirty minutes was only marginally greater than the engineered strains. The agglutinating power of the uninduced MG1655ΔfimA-pPCC1403 strain was very similar to that of the wild-type strain, with the majority of sediments falling out of solution by twenty minutes. From this, it may be deduced that an increase in the level of fimbriation leads to an increased sedimentation rate.

A

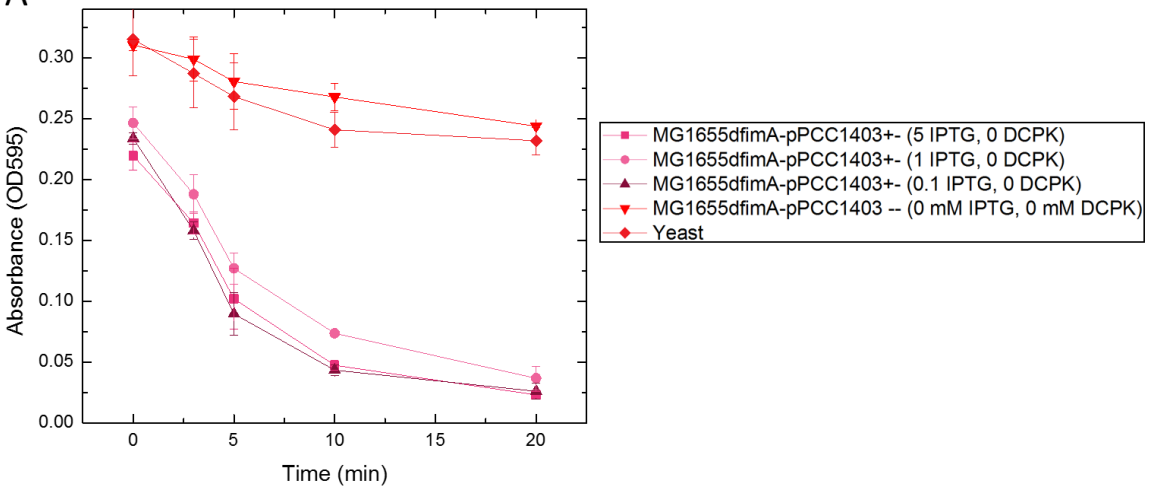
Absorbance (OD595)
0.00
0.05
0.10
0.15
0.20
0.25
0.30
0
5
10
15
20
Time (min)
MG1655dfimA-pPCC1403+- (5 IPTG, 0 DCPK)
MG1655dfimA-pPCC1403+- (1 IPTG, 0 DCPK)
MG1655dfimA-pPCC1403+- (0.1 IPTG, 0 DCPK)
MG1655dfimA-pPCC1403 -- (0 mM IPTG, 0 mM DCPK)
Yeast

B

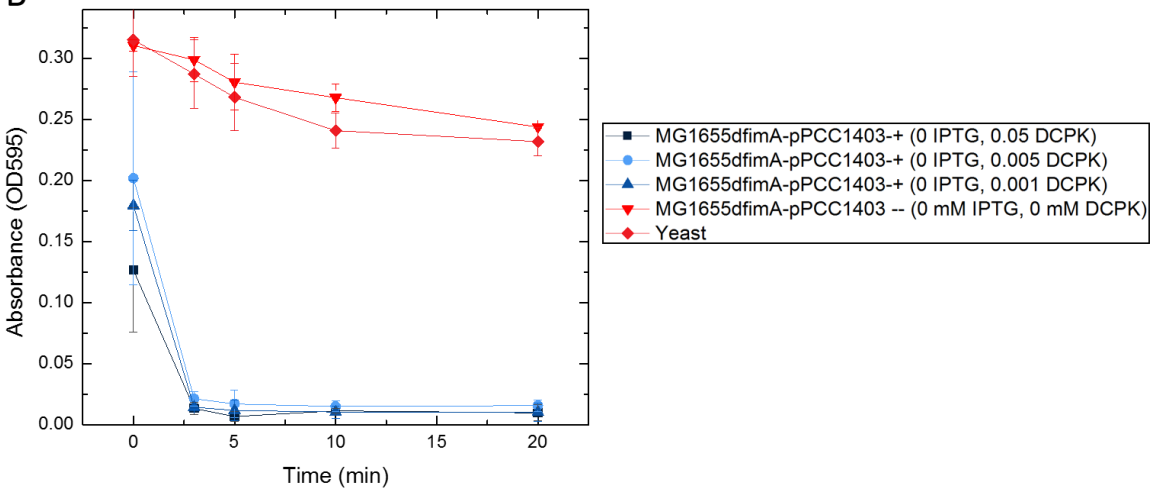
Absorbance (OD595)
0.00
0.05
0.10
0.15
0.20
0.25
0.30
0
5
10
15
20
Time (min)
MG1655dfimA-pPCC1403-+ (0 IPTG, 0.05 DCPK)
MG1655dfimA-pPCC1403-+ (0 IPTG, 0.005 DCPK)
MG1655dfimA-pPCC1403-+ (0 IPTG, 0.001 DCPK)
MG1655dfimA-pPCC1403 -- (0 mM IPTG, 0 mM DCPK)
Yeast

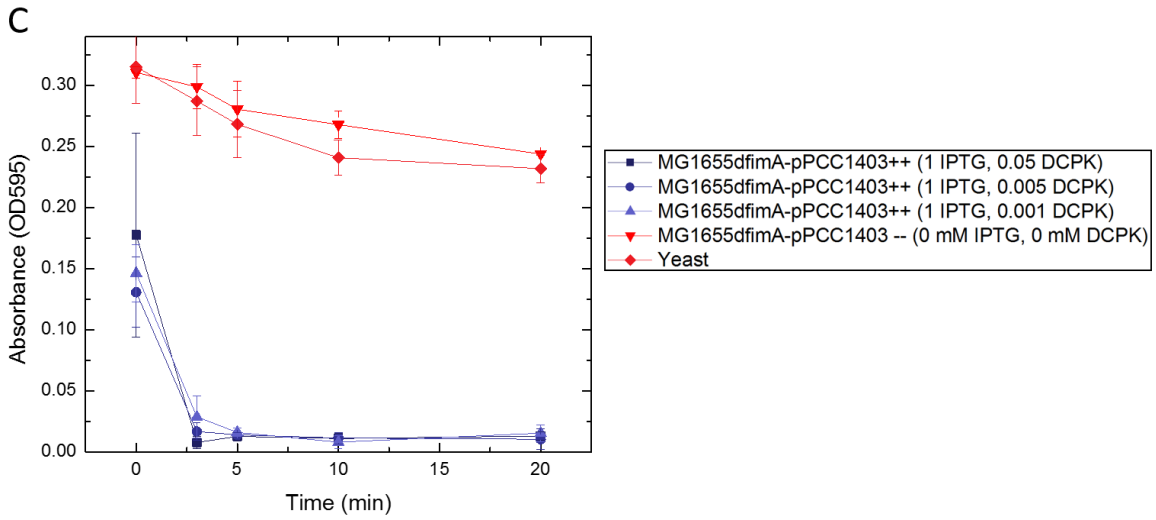

Figure 27: Yeast agglutination assay (YAA), measuring absorbance as a function of time for MG1655ΔfimA-pPCC1403 in the presence inducers IPTG and DCPK across separate ranges of inducer concentrations: variable IPTG, no DCPK (A), no IPTG, variable DCPK (B), and constant IPTG, variable DCPK (C).

Next, we attempted to optimize effects of varying the concentrations of inducers for MG1655ΔfimA-pPCC1403 was studied. For a fixed concentration of IPTG, there was no distinguishably higher agglutinating ability by MG1655ΔfimA-pPCC1403 noticed with lower concentrations of the model-alkane inducer DCPK. Likewise, the effect of the change in concentration of DCPK with no IPTG showed no increase in sedimentation rate as DCPK concentration increased (Fig. 27B). When keeping the concentration of IPTG constant, there was no significant difference in sedimentation rate with increasing concentrations of DCPK (Fig. 27C); there was no statistical difference in sedimentation rate for the case of constant DCPK concentration and varying IPTG concentration. Figure 27A showed that the relatively rapid initial sedimentation rate observed with almost any level of DCPK was no longer maintained when only IPTG inducer was present; the engineered strain was much more dependent on DCPK for induction than IPTG. The sedimentation rate observed in MG1655ΔfimA-pPCC1401 did not depend on the concentration of IPTG. Furthermore, none of the controls (wild-type MG1655; induced

and uninduced MG1655ΔfimA-pFG28A, which contains the parent vector of pPCC1403; uninduced MG1655ΔfimA-pPCC1403; and yeast suspension) exhibited the rapid initial sedimentation rate of MG1655ΔfimA-pPCC1403 in the presence of both IPTG and DCPK or MG1655ΔfimA-pPCC1401 in the presence of IPTG. Such results, biologically, indicate the presence of fimbriae on these induced strains – which bind to mannose-containing substrates.

5.2.3 Specific Biofilm Formation (SBF)

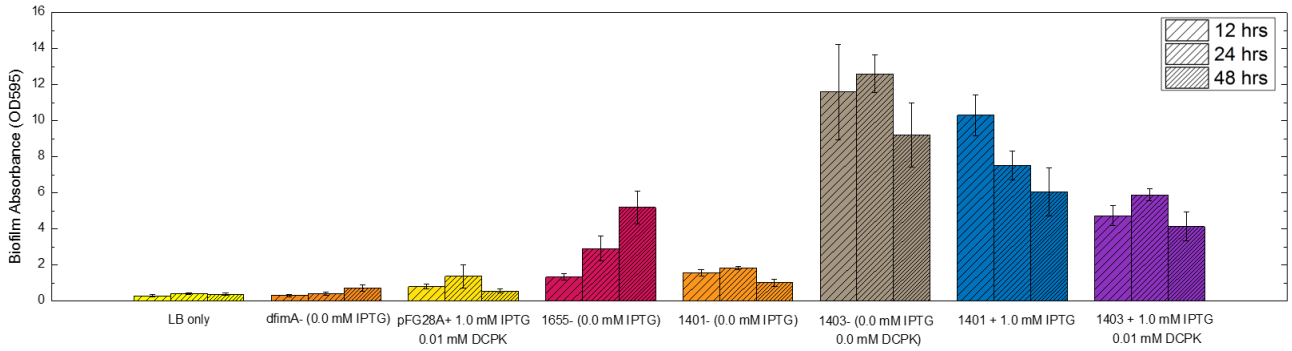

Figure 28: 96-well plate biofilm formation assay, measuring the absorbance of crystal violet (CV) stained biofilms as a function of time. For each sample, biofilm absorbance was measured at 12 h (sparsely shaded), 24 h (medium shading), and 48 h (dense shading). The engineered strain MG1655ΔfimA-pPCC1403 developed the highest amount of biofilm.

To test the biofilm forming ability of all bacterial strains and in all inducer conditions, we measured the overall and absolute biofilm formation using the crystal violet staining assay described in Section 4.2.3. The highest overall biofilm formation was measured in non-induced MG1655ΔfimA-pPCC1403, followed by (in decreasing order) induced MG1655ΔfimA-pPCC1401; induced MG1655ΔfimA-pPCC1403; wild-type MG1655; and non-induced MG1655ΔfimA-pPCC1401 (Figure 28). The amount of biofilm formed by MG1655ΔfimA and MG1655ΔfimA-pFG28A was slightly higher than the film formed in control sample wells that contained only LB growth media, signifying

that the parent plasmid did not aid in biofilm formation. The overall biofilm forming rate did not always increase with increasing incubation time.

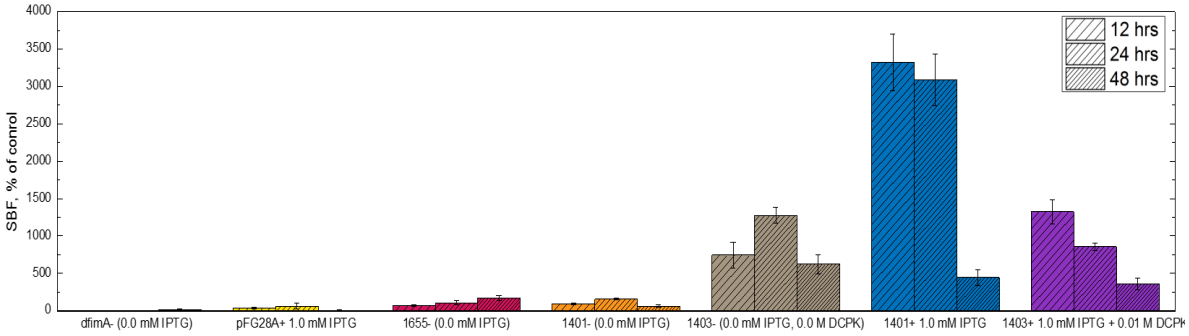

Figure 29: Specific Biofilm Formation (SBF) assay, measuring the absorbance of crystal violet stained biofilms as a function of time and semi-normalized to bacterial growth. For each sample, SBF absorbance was measured at 12 h (sparsely shaded), 24 h (medium shading), and 48 h (dense shading). The engineered strain MG1655ΔfimA-pPCC1401 developed a higher SBF compared to MG1655ΔfimA-pPCC1403, which was much higher than any of the controls.

By normalizing the total biofilm formation of each sample to the cellular growth rate of each well, we measured the specific biofilm formation (SBF) for each set of strain + inducer concentrations. The SBF provide a much more truthful representation of biofilm formed relative to cell growth. The IPTG inducible strain MG1655ΔfimA-pPCC1401 showed the highest levels of specific biofilm formation for all time points, and the SBF decreased with increasing incubation period (Figure 29). The non-induced MG1655ΔfimA-pPCC1403 showed similar levels of specific biofilm formation compared to the induced strain; however, the trend of decreasing SBF with increasing time was only evident in the induced MG1655ΔfimA-pPCC1403 (induced by 1 mM IPTG and 0.01 mM DCPK). The specific biofilm formation levels of non-induced MG1655ΔfimA-pPCC1401, MG1655 wild-type, MG1655ΔfimA, and MG1655ΔfimA-pFG28A were much lower compared to the afore mentioned samples. This increased SBF is associated with increased level of cellular fimbriation.

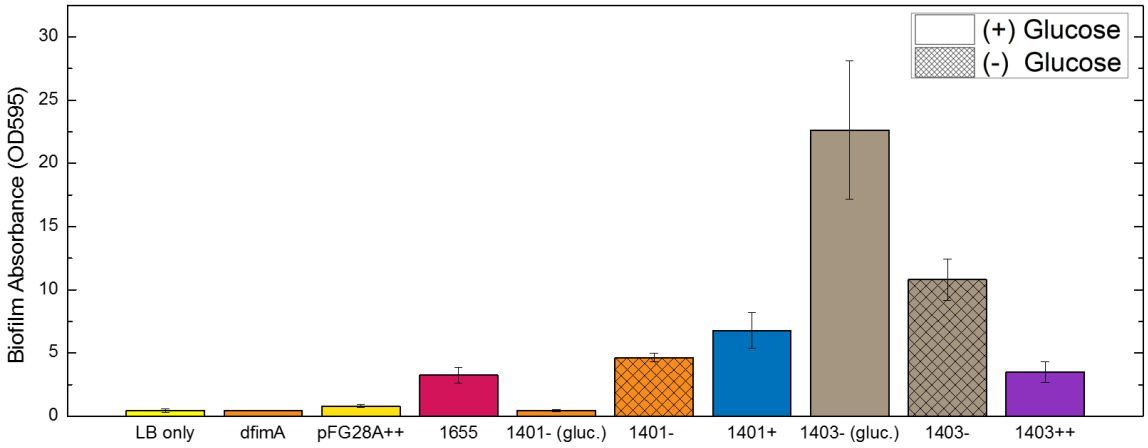

Figure 30: 96-well plate biofilm formation assay, measuring the absorbance of crystal violet (CV) stained biofilms as a function of time. For each sample, biofilm absorbance was measured at 12 h (sparsely shaded), 24 h (medium shading), and 48 h (dense shading). The engineered strain MG1655ΔfimA-pPCC1403 grown with glucose developed the highest total amount of biofilm.

As an attempt to reduce the leaky expression of fimbriae in non-induced MG1655ΔfimA-pPCC1403 samples, we added glucose to all strains and characterized the extent of biofilm formation. Addition of glucose to non-induced MG1655ΔfimA-pPCC1401 greatly reduced biofilm formation, as also observed in earlier samples. In sharp contrast, addition of glucose to non-induced MG1655ΔfimA-pPCC1403 samples did not decrease biofilm formation; instead, biofilm formation of non-induced MG1655ΔfimA-pPCC1403 significantly increased. The biofilm formation of MG1655ΔfimA, MG1655ΔfimA-pFG28A, and non-induced MG1655ΔfimA-pPCC1401 (with glucose addition) were indistinguishable from that in control wells containing only LB growth media (Fig. 30).

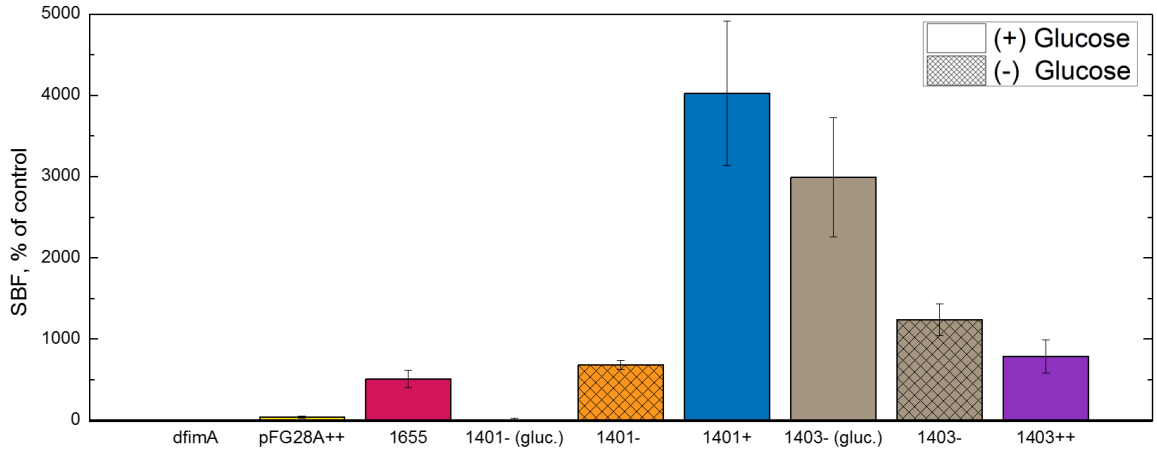

Figure 31: Specific Biofilm Formation (SBF) assay, measuring the absorbance of CV stained biofilms as a function of time and semi-normalized to bacterial growth. For each sample, SBF absorbance was measured at 12 h (sparsely shaded), 24 h (medium shading), and 48 h (dense shading). The engineered strain MG1655ΔfimA-pPCC1401 developed the highest SBF, however, MG1655ΔfimA-pPCC1403 in the presence of glucose developed a SBF close to that of MG1655ΔfimA-pPCC1401.

The specific biofilm formation of all samples was calculated based on equation 3.3 in section 3.4. The IPTG inducible MG1655ΔfimA-pPCC1401 showed the highest specific biofilm formation (Fig. 31). However, the specific biofilm forming ability of non-induced MG1655ΔfimA-pPCC1403 in the presence of glucose was still quite high, with the second highest SBF level of all samples. The specific biofilm formation of MG1655ΔfimA, MG1655ΔfimA-pFG28A, and non-induced MG1655ΔfimA-pPCC1401 (with glucose) were too low to be measurable.

5.3 Results and Discussion

In chapter four, a novel strain of *E. coli* harboring the genetic information requisite of fimbrial expression was engineered (MG1655ΔfimA-pPCC1401). This strain, however, was engineered for induction by IPTG, which is expensive, non-metabolizable, and toxic to cells.[82] The goal of this chapter was to engineer a strain of *E. coli* over expressing fimbriation that was inducible by a chemically relevant molecule related to bioremediation of hydrocarbons: DCPK (8 carbons). As discussed in Section 3.1.2, the plasmid for

MG1655ΔfimA-pPCC1403 was engineered to produce the AlkS protein (under the control of the leaky P_{tac} promoter). This protein subsequently conjugates to small chain hydrocarbons (C5-C12) to form an alkane-inducible complex that activates the P_{alkB} promoter, finally directing the transcription of *fimA-H* engineered directly downstream of the promoter in the presence of DCPK. The level of fimbriation on the newly-engineered alkane-inducible strain MG1655ΔfimA-pPCC1403 was compared to several different controls, including wild-type MG1655, MG1655ΔfimA, MG1655ΔfimA-pFG28A containing the parent vector of MG1655ΔfimA-pPCC1403, and the previously engineered strain MG1655ΔfimA-pPCC1401. Fimbrial quantification tests were performed and were analogous to those performed in chapter four, including the yeast agglutination assay (YAA) and specific biofilm formation (SBF) assays.

As discussed previously, fimbriae have a unique mannose-recognizing receptor located on the FimH adhesin on the distal tip of each lectin domain. Yeast cell walls are composed of a complex mix of polysaccharides (mannans, galactans, glucans, and chitin), where the outermost layer of the cell wall is composed of various mannoproteins – which are polymers of the individual mannose unit.[83,84] Therefore, when yeast and *E. coli* cells are mixed, the fimbriae present on the outer-membrane of *E. coli* cells should bind to these mannan groups lining the periphery of yeast cells – thus forming a small aggregate. As the number of yeast cells in contact with the fimbrial tip of *E. coli* increase, the size of the cluster will increase – thus forming a larger aggregate. Each subsequent yeast cell bound to the fimbriae of the original *E. coli* substrate provides an additional attachment site for other individual *E. coli* cells to bind to, which in turn provides additional attachment sites for yeast; this binding and attachment may then continue in a cascade to form larger and

larger aggregates. As the size of these aggregates increase, they will sediment out of the yeast and *E. coli* suspension/mixture as a function of the square of the aggregate diameter (Eq. 4.1). The alkane-inducible MG1655ΔfimA-pPCC1403 showed approximately the same sedimentation rate as IPTG inducible MG1655ΔfimA-pPCC1401; control over expression of MG1655ΔfimA-pPCC1403 in absence of inducer molecules, however, was low and exhibited a large degree of leaky expression even in the presence of glucose (Fig. 25). This lack of control can be attributed to the discrepancy between the promoters between the two systems used in MG1655ΔfimA-pPCC1401 and in MG1655ΔfimA-pPCC1403. MG1655ΔfimA-pPCC1401 is induced by a simple de-repression mechanism, which is negatively inducible: the genes are normally repressed (turned off) until the presence of an activator (IPTG) binds to the repressor to inactivate the repressor, disallowing its binding to the operator and activating gene transcription. This mechanism of induction does not require specific sigma factors to be recruited for binding to RNA polymerase (RNAP) to recognize promoter regions/sequences. Conversely, MG1655ΔfimA-pPCC1403 utilizes a traditional promoter sequence (P_{alkB}) that requires un-elucidated sigma factors for the recruitment and recognition of its sequence to initiate gene transcription. This regulatory system is more complex than that used in MG1655ΔfimA-pPCC1401. Moreover, the genes involved in AlkS production and the P_{alkB} promoter are heterologous: they are not normally present in *E. coli* but instead originate from *P. putida*). This unknown RNAP promoter recognition mechanism could give rise to the uncontrolled leaky expression seen in MG1655ΔfimA-pPCC1403; by contrast, in MG1655ΔfimA-pPCC1401, glucose successfully repressed leaky expression of fimbriation. The sedimentation rate of MG1655ΔfimA-pPCC1403 was very similar to

MG1655ΔfimA-pPCC1401, with both exhibiting a significantly higher sedimentation rate than the controlled strains with native levels of fimbrial expression and strains with fimbrial deletions (Fig. 26). These findings suggest that the engineered strain MG1655ΔfimA-pPCC1403 produced much higher numbers of fimbriae, which bind to the mannose specific groups on the outside of yeast cells.

The biofilm forming ability of MG1655ΔfimA-pPCC1403 was studied to observe if the trends measured in MG1655ΔfimA-pPCC1401 were conserved in the alkane-inducible strain; it was expected that a higher biofilm formation occur in strains with more fimbriation (as was the case with MG1655ΔfimA-pPCC1401). Following the methods described in Section 3.4, a 96-well polystyrene plate was used to incubate cells for 12, 24, and 48 hours for biofilm quantification. Because polystyrene is hydrophobic,[85] individual cells may have difficulty attaching to the surface. Due to the hydrophobic tyrosine residues lining the binding pocket of the FimH adhesin, it is hypothesized that bacterial strains containing more fimbriae will attach to the hydrophobic polystyrene wells at a higher rate than non-fimbriated strains. Furthermore, because the presence of fimbriae have been linked to greater rates of biofilm formation, we posited that fimbriated bacteria would bind to wells at a higher rate and also form more biofilm relative to cellular growth. The total biofilm formation of MG1655ΔfimA-pPCC1403 of both induced and non-induced strains was high. However, an unexpected trend was noticed in the non-induced MG1655ΔfimA-pPCC1403 strain: the total biofilm formation was higher in the uninduced strain than in the induced strain. Furthermore, the specific biofilm formation was, within error, the same as that in the induced MG1655ΔfimA-pPCC1403. From this, we can say that MG1655ΔfimA-pPCC1403 had significant leaky expression.

In an attempt to prevent the high levels of leaky expression observed in Section 5.2, glucose was added with the goal of reducing leaky expression of the P_{tac}/lacI promoter/repressor system controlling expression in *alkS* (the same control mechanism used for expression of *fimA-H*). If AlkS production caused this high level of leaky expression, addition of glucose should have greatly reduced it (as did glucose addition to MG1655ΔfimA-pPCC1401 in figure 30). However, repression of uninduced MG1655ΔfimA-pPCC1403 did not occur in the presence of glucose; instead, the significant increase in biofilm absorption suggested that an unknown regulatory system controlling P_{alkB} transcription. Indeed, one possible explanation for this surprising result is that the mechanism of induction differs between MG1655ΔfimA-pPCC1401 and MG1655ΔfimA-pPCC1403 and may involve unknown induction pathways. Furthermore, the fact that biofilms were allowed to form in a relatively uncontrolled media (LB) without a defined carbon source could have initiated a cascade of regulatory transcription factors that led to enhanced leaky expression of the uninduced strain. While native P_{alkB} is under carbon catabolite repression (CCR) in *P. putida*, it is not controlled by CCR in *E. coli*.[86] This suggests that the normal gene repression of various genes in *E. coli* by carbon sources, such as glucose (used to repress MG1655ΔfimA-pPCC1401), no longer hold.

Although our results to date do not demonstrate controlled alkane-inducible expression of fimbriae in MG1655ΔfimA-pPCC1403 in the presence of DCPK, nonetheless greater fimbriation was observed in strains containing the newly constructed plasmid pPCC1403. Increased formation of biofilm due to an increased level of fimbriation does not indicate that the construction of an alkane-inducible strain was a success, as the increase in biofilm formation in the uninduced strain with and without

glucose could have been from homologous recombination of *fimA-H* into the transformed cell line. However, data from the yeast agglutination assay for MG1655ΔfimA-pPCC1403 suggested otherwise. All strains with induction at any level of DCPK tested, however, demonstrated increased agglutinating power, as shown by an initial fast sedimentation rate compared to the control (Fig. 27B,C), whereas assays using only IPTG as an inducer resulted in no noticeably different sedimentation rate to that of the controls (Fig. 27A). This data indicated that fimbriation was not the result from a random plasmid containing the genes necessary for fimbriation, as the presence of both inducers was required for the substantial drop in turbidity observed in the beginning minutes of the assay.

5.4 Conclusion

In chapter four, *E. coli* was genetically engineered to express fimbriation in the presence of IPTG, a convenient, well characterized, and widely used model inducer. However, this inducer is expensive, toxic, and is not a relevant molecule for induction processes related to bioremediation. Therefore, a model inducer molecule related to hydrocarbon contamination was sought to induce expression of fimbriation in our bacterial strains. The alkS/P_{alkB} regulation system present in *P. putida* was cloned and combined with the genetic information for fimbrial expression in MG1655ΔfimA-pPCC1401 to engineer the heterologous MG1655ΔfimA-pPCC1403 strain, which was in principle inducible by various alkanes as well as the model hydrocarbon DCPK (C_8). The production of the transcriptional activator AlkS was placed under control of the IPTG inducible P_{tac}/lacI system at use in MG1655ΔfimA-pPCC1401. AlkS may then form a complex by binding a range of alkanes including the alkane-mimicking molecule DCPK, and hence activating transcription of P_{alkB} to express genes located downstream of the promoter – in

our case, fimbriation. The heterologous combination of these components allowed us to engineer MG1655ΔfimA-pPCC1403, a novel alkane-inducible bacterial strain over-expressing fimbriation.

The ability of MG1655ΔfimA-pPCC1403 to produce fimbriae was measured via the yeast agglutination assay (YAA) and specific biofilm formation (SBF) assay used to quantify the presence of fimbria in MG1655ΔfimA-pPCC1401. The YAA showed that MG1655ΔfimA-pPCC1403 had a very similar ability to MG1655ΔfimA-pPCC1403 to agglutinate yeast cells from a solution. However, MG1655ΔfimA-pPCC1403 had a much higher level of leaky expression than MG1655ΔfimA-pPCC1401, even in the presence of glucose. The leaky expression was especially apparent in the SBF assays, in which uninduced MG1655ΔfimA-pPCC1403 produced similar SBF values to induced MG1655ΔfimA-pPCC1403, and uninduced MG1655ΔfimA-pPCC1403 in the presence of glucose resulted in a SBF value exceeding that of the induced strain. These results suggest that an unknown regulatory system interacts with the heterologous system engineered in MG1655ΔfimA-pPCC1403 in an unexpected way. Nonetheless, regardless of leaky expression, the engineered strains produced more fimbriae than strains without the engineered plasmid; because DCPK was required to induce fimbriation, we concluded that the engineered plasmid was responsible for increased fimbriae. Future assays assessing biofilm formation of these strains should be developed to assess biofilm formation at the same specific point of growth (i.e., grown to the same OD before assessing biofilm development, regardless of the time taken to reach this density). An assay at controlled OD is expected to prevent differences observed that are associated with global regulatory systems that are activated at different cell culture densities.

Chapter 6 Conclusion

6.1 Summary and Conclusion

In this study, we investigated the ability of *Escherichia coli* over expressing fimbriae to bind to mannose, partition into hydrocarbons, and form biofilms on abiotic surfaces. In chapter four, the *fim* operon present in wild type MG1655 was manipulated for expression in a bacterial strain with a fimbrial deletion, MG1655ΔfimA, under control of the P_{tac}/lacI promoter system - inducible by IPTG. In chapter five, fimbrial expression was engineered to occur in the presence of hydrocarbons via the AlkS/P_{alkB} dual-regulatory system, which was inducible by the gratuitous inducer DCPK.

Both systems developed, MG1655ΔfimA-pPCC1401 and MG1655ΔfimA-pPCC1403, demonstrated the ability to agglutinate yeast cells and form biofilms. In this investigation, it was shown that both the agglutinating power as well as the biofilm forming ability of *E. coli* was quite dependent on the presence of fimbriae. The fimbrial adhesin tip protein FimH was shown to be very important in both the binding and attachment of fimbriae to biotically relevant molecules and abiotic substrates, as the addition of a non-metabolizable mannose analog (methyl-α-D-pyrranoside) before the start of each assay resulted in responses similar to control strains with fimbrial deletions.

The first engineered strain, MG1655ΔfimA-pPCC1401, was cloned by amplifying the genes necessary for fimbrial development (*fimACDFGH*) from genomic MG1655. The Ptac promoter system, inducible by Isopropyl β-D-1-thiogalactopyranoside (IPTG), was used to control fimbriation in MG1655ΔfimA-pPCC1401, as the native promoters of fimbriae in MG1655, *fimB* and *fimE*, were regulated by a complex regulatory network of more than twenty effectors. This allowed for the controlled expression of fimbriae in

MG1655ΔfimA-pPCC1401. The ability of MG1655ΔfimA-pPCC1401 to agglutinate yeast cells was significantly higher than the wild-type strain MG1655 or control strains with fimbrial deletions, with the majority of aggregates sedimenting out of solution within the first five minutes (Fig. 17). Additionally, MG1655ΔfimA-pPCC1401 showed a much higher tendency to partition into hydrocarbon fractions compared to wild type and control strains in all samples tested, especially in higher chain length hydrocarbons (section 4.2.2). Furthermore, the presence of fimbriae was shown to be essential in the development of biofilms, where MG1655ΔfimA-pPCC1401 developed significantly higher biofilm formation than wild type MG1655, while strains with fimbrial deletions resulted in almost no biofilm formation at all (Fig. 23). The physical presence of fimbriae was verified via transmission electron microscopy (TEM), where MG1655ΔfimA-pPCC1401 demonstrated significant fimbrial presence at a magnification level comparable to the length scale of an *E. coli* cell, while significant magnification was required to visualize fimbrial presence in wild-type MG1655 (no level of magnification nor number of cells scanned resulted in visualization of fimbriae on ΔfimA strains).

The hydrocarbon inducible strain, MG1655ΔfimA-pPCC1403, was cloned by amplifying *fimACDFGH* from plasmid pPCC1401 which was placed under control by the P_{alkB} promoter. The AlkS/P_{alkB} dual-regulatory system was cloned from pFG28A, where AlkS production was inducible by the P_{tac} promoter present in MG1655ΔfimA-pPCC1401, inducible by IPTG. The AlkS protein then conjugated with the alkane-like gratuitous inducer dicyclopropyl ketone (DCPK) to induce the P_{alkB} promoter, thus expressing *fimACDFGH* downstream of P_{alkB} and causing cellular fimbriation. When compared to the efficacy of MG1655ΔfimA-pPCC1401 to agglutinate yeast cells, MG1655ΔfimA-

pPCC1403 induced with IPTG and DCPK showed the same agglutinating power. However, unlike the well-controlled expression of fimbriae on MG1655ΔfimA-pPCC1401, MG1655ΔfimA-pPCC1403 displayed a large level of leakiness or background expression from P_{alkB} under non-induced conditions (the relative leakiness of P_{alkB} has been noted in other heterologous studies[87]). The uninduced expression of fimbriae in MG1655ΔfimA-pPCC1401 was minimized by the addition of glucose (glucose is the preferred carbon source of *E. coli*, resulting in carbon catabolite repression of the *lacI* system); however, when glucose was added to MG1655ΔfimA-pPCC1403, no reduction in expression level was noted. In fact, when glucose was added in the specific biofilm formation assays, the biofilm development actually increased. Such surprising results have also been noticed by other recombinant systems regulated by P_{alkB}, where the absence of catabolite repression of P_{alkB} in *E. coli* recombinants was described as being fundamentally different from regulation mechanism in the host organism (*P. oleovorans*).[86] Nonetheless, the ability of MG1655ΔfimA-pPCC1403 to express fimbriae and agglutinate yeast cells in the presence of DCPK was significant, as assays induced with only IPTG did not result in the initial sedimentation of yeast aggregates.

6.2 Future Work

While the focus of this study concentrated around the development of fimbriation to enhance the attachment and binding of bacterial cells to substrates for enhanced colonization, survivability, persistence of bacteria in contaminated industrial areas, this was only one tenet of a three-pronged approach to bioremediation. In addition to fimbrial-mediated adhesion and biofilm development in targeted contaminated sites, we suggest the

pursuit of additional studies focused on engineered chemotactic response in *E. coli* to common environmental contaminants as well as the metabolism of targeted chemicals.

6.2.1 Chemotaxis towards Environmental Contaminants

Bacterial chemotaxis is the movement of cells toward or away from a chemical gradient, termed positive and negative chemotaxis, respectively. The movement of cells in response to a chemical gradient allow bacteria to find areas for optimum cellular growth or survival. The chemotaxis of various species of bacteria towards xenobiotic contaminants such as BTEX, PAHs, and alkanes has been observed in several species.[88–92] Therefore, we propose the construction of clones containing the genes responsible for chemotaxis towards common pollutants for introduction into *E. coli* for controlled manipulation and modification of genetic components in response to desired chemoeffectors.

The process of chemotaxis is mediated by a two component regulatory system consisting of a histidine kinase and a response regulating protein. When a chemoeffector binds to a chemoreceptor, a confirmation change occurs, modulating kinase activity, which ultimately creates a phosphorylated response regulator protein (CheY) which fuels the motion of the flagellar motor requires for bacterial swimming.[93] The directionality of the flagellar motor dictates the movement of bacteria; in *E. coli*, clockwise (CW) motion leads to bacterial tumbling and counter-clockwise (CCW) motion leads to run cycles of bacterial propulsion.[94–96] Other chemotaxis driven swimming patterns such as run-and-reverse have also been noted, especially in ocean-dwelling bacterial species.[97,98]

The quantification of bacterial chemotaxis to either chemoattractants or chemorepellents may be measured via many methods including colony forming unit (CFU)

assays or microscopy-based methods. The two simplest and most widely used methods of chemotaxis quantification and qualification include the capillary tube assay and agarose plug assay. In the quantitative capillary tube assay, a chemoeffector solution in minimal media is introduced to a dilute cell suspension for a short time (ten minutes), after which the solution is introduced to agar plates and counted for CFUs.[88] The qualitative agarose plug assays use low melting temperature agarose combined with a chemoeffector to observe cellular accumulation around the agarose plug (which may also be conducted in a capillary tube).[92] More advanced methods of chemotactic quantification involve various microfluidic devices with source and sink channels flanking a static well containing cells to generate chemical gradients that may be used to observe the visual migration of cells towards or away from chemoeffectors.[99–101] Such microfluidic devices may be used to calculate the chemotactic sensitivity coefficient and chemotactic receptor constant, which measure the directed bacterial movement due to a chemotactic response and bacterial ability to bind chemoeffectors to its own chemoreceptors, respectively.[102]

6.2.2 Metabolism of Environmental Contaminants

While *Escherichia coli* is the most well-studied bacterial species with a well-understood cellular metabolism and regulatory systems (along with a plethora of genetic tools for modification and amplification of gene expression), in terms of genes required for degradation of many common pollutants, it is deficient. Contrariwise, many bacterial species with known genes for the metabolism of chemicals (such as Pseudomonad spp.), but have less understood regulatory systems. It is for this reason that we suggest the exploration of a third leg in the path towards bioremediation: introduction of heterologous genes in *E. coli* for the metabolism of environmental contaminants. By combining the

well-understood regulatory and metabolic systems in *E. coli* with heterologous genes from outside species that degrade common pollutants, we hope to uncover the essential genes implicated in metabolism of chemicals and elucidating the regulatory systems controlling them. These genes and pathways may then be further explored for improvement in degradation efficiencies. Uncovering such information will allow for the intelligent design of metabolic systems for the degradation of targeted environmental contaminants.

As discussed in section 2.4, the *tod* operon and TOL plasmid are some of the most widely studied gene fragment for degradation of toluene and BTEX derivatives.[103] Future metabolic work concerning the degradation of aromatic pollutants should focus around the use and manipulation of genes located within these two aromatic degradation pathways. Metabolic research involving degradation of alkane and alkane derivatives should concentrate around alkane degrading genes associated with the OCT plasmid from *P. putida* GPo1, including *alkBFGHJKL* encoding proteins involved in the conversion of alkanes to fatty acids and *alkST* which is the transcriptional regulator for expression of *alkBFGHJKL*.[86,104–106]

References

1. Reissig, J. L. *Microbial Interactions*. (Springer Science & Business Media, 2013).
2. Brinton Jr, C. C., Gemski Jr, P. & Carnahan, J. A new type of bacterial pilus genetically controlled by the fertility factor of E. coli K 12 and its role in chromosome transfer. *Proc. Natl. Acad. Sci. U. S. A.* **52,** 776 (1964).
3. Wolf, D. M. & Arkin, A. P. Fifteen minutes of fim: control of type 1 pili expression in E. coli. *OMICS* **6,** 91–114 (2002).
4. Krasowska, A. & Sigler, K. How microorganisms use hydrophobicity and what does this mean for human needs? *Front. Cell. Infect. Microbiol.* **4,** 112 (2014).
5. Thomas, W. E., Trintchina, E., Forero, M., Vogel, V. & Sokurenko, E. V. Bacterial adhesion to target cells enhanced by shear force. *Cell* **109,** 913–923 (2002).
6. Andersson, S. *Characterization of Bacterial Biofilms for Wastewater Treatment*. *Technology* (2009).
7. Van Houdt, R. & Michiels, C. W. Role of bacterial cell surface structures in Escherichia coli biofilm formation. *Res. Microbiol.* **156,** 626–633 (2005).
8. Danese, P. N., Pratt, L. A. & Kolter, R. Exopolysaccharide production is required for development of *Escherichia coli* K-12 biofilm architecture. *J. Bacteriol.* **182,** 3593–3596 (2000).
9. Donlan, R. M. Biofilms: Microbial life on surfaces. *Emerg. Infect. Dis.* **8,** 881–890 (2002).
10. Vu, B., Chen, M., Crawford, R. J. & Ivanova, E. P. Bacterial extracellular polysaccharides involved in biofilm formation. *Molecules* **14,** 2535–2554 (2009).
11. Singh, T., Saikia, R., Jana, T. & Arora, D. K. Hydrophobicity and surface

electrostatic charge of conidia of the mycoparasitic Trichoderma species. *Mycol. Prog.* **3,** 219–228 (2004).

12. Wellens, A., Lahmann, M., Touaibia, M., Vaucher, J., Oscarson, S., Roy, R., Remaut, H. & Bouckaert, J. The tyrosine gate as a potential entropic lever in the receptor-binding site of the bacterial adhesin FimH. *Biochemistry* **51,** 4790–4799 (2012).
13. Morisaki, H., Nagai, S., Ohshima, H., Ikemoto, E. & Kogure, K. The effect of motility and cell-surface polymers on bacterial attachment. *Microbiology* **145,** 2797–2802 (1999).
14. Reisner, A., Haagensen, J. A. J., Schembri, M. A., Zechner, E. L. & Molin, S. Development and maturation of Escherichia coli K-12 biofilms. *Mol. Microbiol.* **48,** 933–946 (2003).
15. Rodrigues, D. F. & Elimelech, M. Role of type 1 fimbriae and mannose in the development of Escherichia coli K12 biofilm: from initial cell adhesion to biofilm formation. *Biofouling* **25,** 401–11 (2009).
16. US EPA, O. O. Superfund: National Priorities List (NPL).
17. Agency, E. P., Waste, S., Response, E. & Offlce, T. I. Cleaning Up the Nation ' S Waste Sites : Markets and Technology Trends. (1993).
18. Godleads Omokhagbor Adams, Prekeyi Tawari Fufeyin, Samson Eruke Okoro, I. E. Bioremediation, Biostimulation and Bioaugmention: A Review. *Int. J. Environ. Bioremediation Biodegrad.* **3,** 28–39 (2015).
19. Magesh, H., Kumar, A., Alam, A., Priyam, Sekar, U., Sumantran, V. N. & Vaidyanathan, R. Identification of natural compounds which inhibit biofilm

formation in clinical isolates of Klebsiella pneumoniae. *Indian J. Exp. Biol.* **51,** 764–772 (2013).

20. Sepandj, F., Ceri, H., Gibb, A., Read, R. & Olson, M. Minimum inhibitory concentration versus minimum biofilm eliminating concentration in evaluation of antibiotic sensitivity of enterococci causing peritonitis [1]. *Perit. Dial. Int.* **27,** 464–465 (2007).

21. Ceri, H., Olson, M. E., Stremick, C., Read, R. R., Morck, D. & Buret, A. The Calgary Biofilm Device: New technology for rapid determination of antibiotic susceptibilities of bacterial biofilms. *J. Clin. Microbiol.* **37,** 1771–1776 (1999).

22. Wojnicz, D. & Tichaczek-Goska, D. Effect of sub-minimum inhibitory concentrations of ciprofloxacin, amikacin and colistin on biofilm formation and virulence factors of Escherichia coli planktonic and biofilm forms isolated from human urine. *Brazilian J. Microbiol.* **44,** 259–265 (2013).

23. Burns, L. S., Smith, S. G. J. & Dorman, C. J. Interaction of the FimB integrase with the fimS invertible DNA element in Escherichia coli in vivo and in vitro. *J. Bacteriol.* **182,** 2953–2959 (2000).

24. Xie, Y., Yao, Y., Kolisnychenko, V., Teng, C. H. & Kim, K. S. HbiF regulates type 1 fimbriation independently of FimB and FimE. *Infect. Immun.* **74,** 4039–4047 (2006).

25. Schwan, W. R. Regulation of *fim* genes in uropathogenic *Escherichia coli*. *World J. Clin. Infect. Dis.* **1,** 17–25 (2011).

26. Schilling, J. D., Mulvey, M. A., & Hultgren, S. J. Structure and Function of Escherichia coli Type 1 Pili: New Insight into the Pathogenesis of Urinary Tract

Infections. *Journal of Infectious Diseases*. **183**, S36-40.

27. Waksman, G. & Hultgren, S. J. Structural biology of the chaperone-usher pathway of pilus biogenesis. *Nat. Rev. Microbiol.* **7,** 765–74 (2009).

28. Pratt, L. a & Kolter, R. Genetic analyses of bacterial biofilm formation. *Curr. Opin. Microbiol.* **2,** 598–603 (1999).

29. Pratt, L. A. & Kolter, R. Genetic analysis of Escherichia coli biofilm formation: Roles of flagella, motility, chemotaxis and type I pili. *Mol. Microbiol.* **30,** 285–293 (1998).

30. Sauer, M. M., Jakob, R. P., Eras, J., Baday, S., Eris, D., Navarra, G., Ernst, B., Maier, T. & Glockshuber, R. Catch-bond mechanism of the bacterial adhesin FimH. (2016). doi:10.1038/ncomms10738

31. Aprikian, P., Tchesnokova, V., Kidd, B., Yakovenko, O., Yarov-Yarovoy, V., Trinchina, E., Vogel, V., Thomas, W. & Sokurenko, E. Interdomain interaction in the FimH adhesin of Escherichia coli regulates the affinity to mannose. *J. Biol. Chem.* **282,** 23437–23446 (2007).

32. Stahlhut, S. G., Tchesnokova, V., Struve, C., Weissman, S. J., Chattopadhyay, S., Yakovenko, O., Aprikian, P., Sokurenko, E. V. & Krogfelt, K. A. Comparative structure-function analysis of mannose-specific FimH adhesins from Klebsiella pneumoniae and Escherichia coli. *J. Bacteriol.* **191,** 6592–6601 (2009).

33. Loris, R., Hamelryck, T., Bouckaert, J. & Wyns, L. Legume lectin structure. *Biochim. Biophys. Acta - Protein Struct. Mol. Enzymol.* **1383,** 9–36 (1998).

34. Wellens, A., Garofalo, C., Nguyen, H., Van Gerven, N., Sl??ttegard, R., Hernalsteens, J. P., Wyns, L., Oscarson, S., De Greve, H., Hultgren, S. & Bouckaert,

J. Intervening with urinary tract infectious using anti-adhesives based on the crystal structure of the FimH-oligomannose-3 complex. *PLoS One* **3,** (2008).

35. Sharon, N. & Lis, H. *Lectins*. (Springer Science & Business Media, 2003).

36. Marshall, K. C., Stout, R. & Mitchell, R. Mechanism of the Initial Events in the Sorption of Marine Bacteria to Surfaces. *J. Gen. Microbiol.* **68,** 337–348 (1971).

37. Bennett, K. M., Walker, S. L. & Lo, D. D. Epithelial microvilli establish an electrostatic barrier to microbial adhesion. *Infect. Immun.* **82,** 2860–2871 (2014).

38. Rodrigues, D. F. and Elimelech, M. Role of type 1 fimbriae and mannose in the development of Escherichia coli K12 biofilm: from initial cell adhesion to biofilm formation.Biofouling. **25**, 401-411 (2009).

39. Guiton, P. S., Cusumano, C. K., Kline, K. A., Dodson, K. W., Han, Z., Janetka, J. W., Henderson, J. P., Caparon, M. G. & Hultgren, S. J. Combinatorial small-molecule therapy prevents uropathogenic Escherichia coli catheter-associated urinary tract infections in mice. *Antimicrob. Agents Chemother.* **56,** 4738–4745 (2012).

40. Trautner, B. W., Cevallos, M. E., Li, H., Riosa, S., Hull, R. a, Hull, S. I., Tweardy, D. J. & Darouiche, R. O. Increased expression of type-1 fimbriae by nonpathogenic Escherichia coli 83972 results in an increased capacity for catheter adherence and bacterial interference. *J. Infect. Dis.* **198,** 899–906 (2008).

41. Rockne, K. J. & Reddy, K. R. Bioremediation of Contaminated Sites. *Int. e-Conference Mod. Trends Found. Eng. Geotech. Challenges Solut.* 1–22 (2003).

42. States, U., Waste, S. & Response, E. Use of Bioremediation at Use of Bioremediation at Superfund Sites. 6–13 (2001).

43. Weiner, J. M. & Lovley, D. R. Rapid Benzene Degradation in Methanogenic Sediments from a Petroleum-Contaminated Aquifer Rapid Benzene Degradation in Methanogenic Sediments from a Petroleum-Contaminated Aquifer. *Appl. Environ. Microbiol.* **64,** 1937–1939 (1998).

44. Duque, E., Haidour, A., Godoy, F. & Ramos, J. L. Construction of a Pseudomonas hybrid strain that mineralizes 2,4,6- trinitrotoluene. *J. Bacteriol.* **175,** 2278–2283 (1993).

45. Hawari, J., Halasz, A., Beaudet, S., Paquet, L., Ampleman, G. U. Y. & Thiboutot, S. chrysosporium in Agitated Cultures at pH 4 . 5 †. **65,** 2977–2986 (1999).

46. Wild, a, Hermann, R. & Leisinger, T. Isolation of an anaerobic bacterium which reductively dechlorinates tetrachloroethene and trichloroethene. *Biodegradation* **7,** 507–511 (1997).

47. Ackerley, D. F., Gonzalez, C. F., Keyhan, M., Blake, R. & Matin, A. Mechanism of chromate reduction by the Escherichia coli protein, NfsA, and the role of different chromate reductases in minimizing oxidative stress during chromate reduction. *Environ. Microbiol.* **6,** 851–860 (2004).

48. Hyun, S., Dissertations, P. & Text, T. F. Engineered Escherichia coli and its application in bioremediation and nanotechnology. (2009).

49. Wilson, D. B. Construction and characterization of Escherichia coli genetically engineered for Construction and Characterization of Escherichia coli Genetically Engineered for Bioremediation of Hg 2 ∂ -Contaminated Environments. **63,** 2–6 (1997).

50. D.M., A., Reguera, B., Pitcher, G. C. & Enevoldsen, H. O. Deep Water Horizon Oil

Spill A review of the Planktonic response. *Oceanography* **24,** 162–173 (2011).

51. Zein, M. M., Pinto, P. X., Garcia-Blanco, S., Suidan, M. T. & Venosa, A. D. Treatment of groundwater contaminated with PAHs, gasoline hydrocarbons, and methyl tert-butyl ether in a laboratory biomass-retaining bioreactor. *Biodegradation* **17,** 57–69 (2006).

52. Díaz, E., Ferrández, A., Prieto, M. a & García, J. L. Biodegradation of aromatic compounds by Escherichia coli. *Microbiol. Mol. Biol. Rev.* **65,** 523–569, table of contents (2001).

53. Lin, Y. & Cai, L. X. PAH-degrading microbial consortium and its pyrene-degrading plasmids from mangrove sediment samples in Huian, China. *Mar. Pollut. Bull.* **57,** 703–706 (2008).

54. Obayori, O. S. & Salam, L. B. Degradation of polycyclic aromatic hydrocarbons : Role of plasmids. *Sci. Res. Essays* **5,** 4093–4106 (2010).

55. Zylstra, G. J. & Gibson, D. T. Toluene degradation by Pseudomonas putida F1. Nucleotide sequence of the todC1C2BADE genes and their expression in Escherichia coli. *J. Biol. Chem.* **264,** 14940–14946 (1989).

56. Zylstra, G. J., McCombie, W. R., Gibson, D. T. & Finette, B. A. Toluene degradation by Pseudomonas putida F1: genetic organization of the tod operon. *Appl. Environ. Microbiol.* **54,** 1498–1503 (1988).

57. Kasai, Y., Inoue, J. & Harayama, S. The TOL Plasmid pWW0 xylN Gene Product from Pseudomonas putida Is Involved in m- Xylene Uptake The TOL Plasmid pWW0 xylN Gene Product from Pseudomonas putida Is Involved in m- Xylene Uptake. **183,** 6662–6666 (2001).

58. Franklin, F. C., Bagdasarian, M., Bagdasarian, M. M. & Timmis, K. N. Molecular and functional analysis of the TOL plasmid pWWO from Pseudomonas putida and cloning of genes for the entire regulated aromatic ring meta cleavage pathway. *Proc. Natl. Acad. Sci. U. S. A.* **78,** 7458–7462 (1981).

59. Mermod, N., Lehrbach, P. R., Reineke, W. & Timmis, K. N. Transcription of the TOL plasmid toluate catabolic pathway operon of Pseudomonas putida is determined by a pair of co-ordinately and positively regulated overlapping promoters. *EMBO J.* **3,** 2461–6 (1984).

60. Gibson, D. T., Davey, J. F. & Mahadevan, V. of the Aromatic Ring Bacterial Metabolism of para- and meta-Xylene : Oxidation of the Aromatic Ring. **119,** 930–936 (1974).

61. Worsey, M. J. & Williams, P. A. Metabolism of toluene and xylenes by Pseudomonas (putida (arvilla) mt-2: evidence for a new function of the TOL plasmid. *J. Bacteriol.* **124,** 7–13 (1975).

62. Lee, J. Y., Jung, K. H., Sang Ho Choi & Kim, H. S. Combination of the tod and the tol pathways in redesigning a metabolic route of Pseudomonas putida for the mineralization of a benzene, toluene, and p-xylene mixture. *Appl. Environ. Microbiol.* **61,** 2211–2217 (1995).

63. Zylstra, G. J., Wackett, L. P. & Gibson, D. T. Trichloroethylene degradation by Escherichia coli containing the cloned Pseudomonas putida F1 toluene dioxygenase genes. *Appl. Environ. Microbiol.* **55,** 3162–3166 (1989).

64. Furukawa, K., Hirose, J., Suyama, A., Zainki, T. & Hayashida, S. Gene components responsible for discrete substrate specificity in the metabolism of biphenyl (bph

operon) and toluene (tod operon). *J. Bacteriol.* **175,** 5224–5232 (1993).

65. Egland, P. G., Pelletier, D. a, Dispensa, M., Gibson, J. & Harwood, C. S. A cluster of bacterial genes for anaerobic benzene ring biodegradation. *Proc. Natl. Acad. Sci. U. S. A.* **94,** 6484–6489 (1997).

66. Lee, J. H., Regmi, S. C., Kim, J. A., Cho, M. H., Yun, H., Lee, C. S. & Lee, J. Apple flavonoid phloretin inhibits Escherichia coli O157:H7 biofilm formation and ameliorates colon inflammation in rats. *Infect. Immun.* **79,** 4819–4827 (2011).

67. Niu, C. & Gilbert, E. S. Colorimetric Method for Identifying Plant Essential Oil Components That Affect Biofilm Formation and Structure. *Society* **70,** 6951–6956 (2004).

68. Bouckaert, J., Mackenzie, J., De Paz, J. L., Chipwaza, B., Choudhury, D., Zavialov, A., Mannerstedt, K., Anderson, J., Piérard, D., Wyns, L., Seeberger, P. H., Oscarson, S., De Greve, H. & Knight, S. D. The affinity of the FimH fimbrial adhesin is receptor-driven and quasi-independent of Escherichia coli pathotypes. *Mol. Microbiol.* **61,** 1556–1568 (2006).

69. Perry, A., Ofek, I. & Silverblatt, F. J. Enhancement of mannose-mediated stimulation of human granulocytes by type 1 fimbriae aggregated with antibodies on Escherichia coli surfaces. *Infect. Immun.* **39,** 1334–1345 (1983).

70. Eshdat, Y., Speth, V. & Jann, K. Participation of pili and cell wall adhesion in the yeast agglutination activity of Escherichia coli. *Infect. Immun.* **34,** 980–986 (1981).

71. Eshdat, Y., Ofek, I., Yashouv-Gan, Y., Sharon, N. & Mirelman, D. Isolation of a mannose-specific lectin from Escherichia coli and its role in the adherence of the bacteria to epithelial cells. *Biochem. Biophys. Res. Commun.* **85,** 1551–1559 (1978).

72. Blumer, C., Kleefeld, A., Lehnen, D., Heintz, M., Dobrindt, U., Nagy, G., Michaelis, K., Emody, L., Polen, T., Rachel, R., Wendisch, V. F. & Unden, G. Regulation of type 1 fimbriae synthesis and biofilm formation by the transcriptional regulator LrhA of Escherichia coli. *Microbiology* **151,** 3287–3298 (2005).

73. van der Mei, H. C., van de Belt-Gritter, B. & Busscher, H. J. Implications of microbial adhesion to hydrocarbons for evaluating cell surface hydrophobicity 2. Adhesion mechanisms. *Colloids Surfaces B Biointerfaces* **5,** 117–126 (1995).

74. Pembrey, R. S. & Marshall, K. C. Cell Surface Analysis Techniques : What Do Cell Preparation Protocols Do to Cell Surface Properties ? **65,** 2877–2894 (1999).

75. Van Der Mei, H. C., Bos, R. & Busscher, H. J. A reference guide to microbial cell surface hydrophobicity based on contact angles. *Colloids Surfaces B Biointerfaces* **11,** 213–221 (1998).

76. Geertsema-Doornbusch, G. I., van der Mei, H. C. & Busscher, H. J. Microbial cell surface hydrophobicity The involvement of electrostatic interactions in microbial adhesion to hydrocarbons (MATH). *J. Microbiol. Methods* **18,** 61–68 (1993).

77. Khanal, M., Larsonneur, F., Raks, V., Barras, A., Baumann, J.-S., Martin, F. A., Boukherroub, R., Ghigo, J.-M., Ortiz Mellet, C., Zaitsev, V., Garcia Fernandez, J. M., Beloin, C., Siriwardena, A. & Szunerits, S. Inhibition of type 1 fimbriae-mediated Escherichia coli adhesion and biofilm formation by trimeric cluster thiomannosides conjugated to diamond nanoparticles. *Nanoscale* **7,** 2325–35 (2015).

78. Vikram, A., Jayaprakasha, G. K., Jesudhasan, P. R., Pillai, S. D. & Patil, B. S. Suppression of bacterial cell-cell signalling, biofilm formation and type III secretion

system by citrus flavonoids. *J. Appl. Microbiol.* **109,** 515–527 (2010).

79. Stepanović, S., Vuković, D., Dakić, I., Savić, B. & Švabić-Vlahović, M. A modified microtiter-plate test for quantification of staphylococcal biofilm formation. *J. Microbiol. Methods* **40,** 175–179 (2000).

80. Li, Y., Lau, P. C. Y., Lee, J. H., Ellen, R. P. & Cvitkovitch, D. G. Natural Genetic Transformation of Streptococcus mutans Growing in Biofilms Natural Genetic Transformation of Streptococcus mutans Growing in Biofilms. *Society* **183,** 897–908 (2001).

81. Djordjevic, D. Microtiter plate assay for assessment of Listeria monocytogenes biofilm formation. *Appl. Environ. Microbiol.* **68,** 2950–2958 (2002).

82. Vélez, A. M., da Silva, A. J., Luperni Horta, A. C., Sargo, C. R., Campani, G., Gonçalves Silva, G., de Lima Camargo Giordano, R. & Zangirolami, T. C. High-throughput strategies for penicillin G acylase production in rE. coli fed-batch cultivations. *BMC Biotechnol.* **14,** 6 (2014).

83. Lesage, G. & Bussey, H. Cell wall assembly in Saccharomyces cerevisiae. *Microbiol. Mol. Biol. Rev.* **70,** 317–43 (2006).

84. Cummings, R. D. & Doering, T. L. Fungi. (2009).

85. Surface, C. C. Technical Appendix Corning® Cell Culture Surfaces. 47–49

86. Staijen, I. E., Marcionelli, R. & Witholt, B. The P alkBFGHJKL Promoter Is under Carbon Catabolite Repression Control in Pseudomonas oleovorans but Not in Escherichia coli alk + Recombinants The P alkBFGHJKL Promoter Is under Carbon Catabolite Repression Control in Pseudomonas oleovorans but Not in E. **181,** 1610–1616 (1999).

87. Sticher, P., Jaspers, M. C. M., Stemmler, K., Harms, H., Zehnder, A. J. B. & Van Der Meer, J. R. Development and characterization of a whole-cell bioluminescent sensor for bioavailable middle-chain alkanes in contaminated groundwater samples. *Appl. Environ. Microbiol.* **63,** 4053–4060 (1997).

88. Lacal, J., Munoz-Martinez, F., Reyes-Darias, J. A., Duque, E., Matilla, M., Segura, A., Calvo, J. J. O., Jimenez-Sanchez, C., Krell, T. & Ramos, J. L. Bacterial chemotaxis towards aromatic hydrocarbons in Pseudomonas. *Environ. Microbiol.* **13,** 1733–1744 (2011).

89. Grimm, A. C. & Harwood, C. S. Chemotaxis of Pseudomonasspp. to the polyaromatic hydrocarbon naphthalene. *Appl Env. Microbiol* **63,** 4111–4115 (1997).

90. Harwood, C. S., Parales, R. E. & Dispensa, M. Chemotaxis of Pseudomonas putida toward chlorinated benzoates. *Appl. Environ. Microbiol.* **56,** 1501–1503 (1990).

91. Parales, R. E. & Harwood, C. S. Bacterial chemotaxis to pollutants and plant-derived aromatic molecules. *Curr. Opin. Microbiol.* **5,** 266–273 (2002).

92. Parales, R. E., Ditty, J. L., Harwood, C. S. & Harwood, C. S. Toluene-Degrading Bacteria Are Chemotactic towards the Environmental Pollutants Benzene , Toluene , and Trichloroethylene Toluene-Degrading Bacteria Are Chemotactic towards the Environmental Pollutants Benzene , Toluene , and Trichloroethylene. **66,** 4098–4104 (2000).

93. Bi, S. & Lai, L. Bacterial chemoreceptors and chemoeffectors. *Cell. Mol. Life Sci.* **72,** 691–708 (2015).

94. Turner, L., Ryu, W. S. & Berg, H. C. Real-time imaging of fluorescent flagellar filaments. *J. Bacteriol.* **182,** 2793–2801 (2000).

95. Berg, H. C. & Berg, H. C. Ehavior of. *Genet. Anal.* 24–29 (2000).

96. Sourjik, V. & Wingreen, N. S. Responding to chemical gradients: Bacterial chemotaxis. *Curr. Opin. Cell Biol.* **24,** 262–268 (2012).

97. Stocker, R. Reverse and flick: Hybrid locomotion in bacteria. *Proc. Natl. Acad. Sci. U. S. A.* **108,** 2635–2636 (2011).

98. Taktikos, J., Stark, H. & Zaburdaev, V. How the motility pattern of bacteria affects their dispersal and chemotaxis. *PLoS One* **8,** (2013).

99. Ahmed, T., Shimizu, T. S. & Stocker, R. Bacterial chemotaxis in linear and nonlinear steady microfluidic gradients. *Nano Lett.* **10,** 3379–3385 (2010).

100. Diao, J., Young, L., Kim, S., Fogarty, E. a, Heilman, S. M., Zhou, P., Shuler, M. L., Wu, M. & DeLisa, M. P. A three-channel microfluidic device for generating static linear gradients and its application to the quantitative analysis of bacterial chemotaxis. *Lab Chip* **6,** 381–8 (2006).

101. Atencia, J., Cooksey, G. A. & Locascio, L. E. A robust diffusion-based gradient generator for dynamic cell assays. *Lab Chip* **12,** 309–16 (2012).

102. Wang, X., Atencia, J. & Ford, R. M. Quantitative analysis of chemotaxis towards toluene by Pseudomonas putida in a convection-free microfluidic device. *Biotechnol. Bioeng.* **112,** 896–904 (2015).

103. Krell, T., Lacal, J., Guazzaroni, M. E., Busch, A., Silva-Jiménez, H., Fillet, S., Reyes-Darías, J. A., Muñoz-Martínez, F., Rico-Jiménez, M., García-Fontana, C., Duque, E., Segura, A. & Ramos, J. L. Responses of Pseudomonas putida to toxic aromatic carbon sources. *J. Biotechnol.* **160,** 25–32 (2012).

104. van Beilen, J. B., Panke, S., Lucchini, S., Franchini, A. G., Rothlis-berger, M. &

Witholt, B. Analysis of Pseudomonas putida alkane degradation gene clusters and flanking insertion sequences: evolution and regulation of the alk-genes. *Microbiology* **147,** 1621–1630 (2001).

105. Rojo, F. Degradation of alkanes by bacteria: Minireview. *Environ. Microbiol.* **11,** 2477–2490 (2009).

106. Dinamarca, M. A., Aranda-olmedo, I., Puyet, A. & Rojo, F. Expression of the. *Society* **185,** 4772–4778 (2003).